NASA-CR-72229
AI-67-93

TUNGSTEN RESONANCE INTEGRALS AND DOPPLER COEFFICIENTS

FINAL REPORT

Prepared for

NATIONAL AERONAUTICS AND SPACE ADMINISTRATION

LEWIS RESEARCH CENTER

Under Contract No. NAS3-7982

ATOMICS INTERNATIONAL

A DIVISION OF NORTH AMERICAN AVIATION, INC.

NOTICES

This report was prepared as an account of Government-sponsored work. Neither the United States nor the National Aeronautics and Space Administration (NASA), nor any person acting on behalf of NASA:

A) Makes any warranty or representation, expressed or implied, with respect to the accuracy, completeness, or usefulness of the information contained in this report, or that the use of any information, apparatus, method, or process disclosed in this report may not infringe privately-owned rights; or

B) Assumes any liabilities with respect to the use of, or for damage resulting from the use of any information, apparatus, method or process disclosed in this report.

As used above, "person acting on behalf of NASA" includes any employee or contractor of NASA, or employee of such contractor, to the extent that such employee or contractor of NASA or employee of such contractor prepares, disseminates, or provides access to, any information pursuant to his employment or contract with NASA, or his employment with such contractor.

AVAILABILITY NOTICE

Qualified requestors may obtain copies of this report from:

National Aeronautics and Space Administration
Office of Scientific and Technical Information
Washington 25, D.C.
Attn: AFSS-A

NASA-CR-72229
AI-67-93

TUNGSTEN RESONANCE INTEGRALS AND DOPPLER COEFFICIENTS

FINAL REPORT

By

H. N. ROYDEN
R. K. PASCHALL
J. M. OTTER
S. G. CARPENTER

Prepared for
National Aeronautics and Space Administration
Lewis Research Center

Project Management
NASA – Lewis Research Center
Nuclear Reactor Division
R. E. Sullivan

ATOMICS INTERNATIONAL

A DIVISION OF NORTH AMERICAN AVIATION, INC.

CONTRACT: NAS3-7982
ISSUED: JUNE 30, 1967

TUNGSTEN RESONANCE INTEGRALS AND DOPPLER COEFFICIENTS

By

H. N. Royden
R. K. Paschall
J. M. Otter
S. G. Carpenter

Atomics International
A Division of North American Aviation, Inc.

SUMMARY

Measurements of effective resonance integrals and Doppler coefficients of thick samples of natural and enriched tungsten have been performed in a 1/E spectrum with sample temperatures up to 2273 °K and compared with calculated values. Results of the Doppler measurements up to 1370°K clearly favor the $T^{1/2}$ dependence of resonance absorption usually assumed for a 1/E spectrum, where T is the absolute temperature of the absorber. Measurements from 1370 to 2273 °K were made with ovens of a new design, and were less accurate because of large oven-dependent reactivity effects.

The epicadmium reactivity of each sample was determined as a function of temperature in the Sodium Graphite Reactor Critical Assembly (SGR-CA). These reactivities were converted into effective resonance integrals by comparison with epicadmium measurements on samples of gold, which has a well-known effective resonance integral. Reactivities were determined from the reactor power history during repeated cycles of sample insertion and removal, by numerical solution of the reactor-kinetic equations. For Doppler-effect measurements, tungsten samples were heated electrically in evacuated ovens.

Calculations were carried out with a resonance-integral code based on analytical approximations to the neutron slowing-down equation and an improved rational approximation to the escape probability for lumped absorbers. This method overestimated both effective resonance integrals and Doppler coefficients by as much as 25% for some samples. Resonance overlap in natural tungsten and failure of the flat-source approximation in W^{186} can account for most of the resonance-integral overestimates for these two samples. Reasons for the other discrepancies are being investigated; it seems likely that no single effect is responsible.

CONTENTS

CONTENTS

TABLES

TABLES

FIGURES

I. INTRODUCTION

Described in this report are measurements of the Doppler coefficients and effective resonance integrals of samples of natural and isotopically enriched tungsten, with sample temperatures ranging from 295 to 2273°K. Results are compared with predictions made using theoretical methods based on improvements to widely used analytical approximations.

The nuclear Doppler effect is one of the most important mechanisms affecting the dynamic behavior of a reactor. It arises from the increase in neutron absorption in resonances in heavy nuclei caused by thermal motion of these nuclei. If the material involved is a pure absorber, such as U^{238}, a rise in its temperature increases neutron absorption in the reactor, thereby causing a decrease in reactivity. When the absorber is intimately mixed with the fissile material, the reactivity decrease is prompt. Reactors with heavy absorbers in the fuel elements thus possess an inherent mechanism for limiting power surges. In many reactor types, this prompt, negative temperature coefficient of reactivity also contributes substantially to stability under normal operating conditions. The Doppler effect in fissile nuclei can be either negative or positive, the sign depending on the balance between fission and absorption in individual resonances, and therefore on the neutron spectrum. Nearly all reactors have significant Doppler coefficients; only in small, highly enriched fast reactors will the neutron spectrum be concentrated at such high energies that no appreciable fraction of the neutron population will have energies in the resonance region (approximately 1 to 10^5 ev, although most of the Doppler effect is contributed by resonances below 10 kev).

The original and best-known "Doppler effect" is, of course, the change in apparent frequency of a sound wave caused by relative motion between source and observer. The nuclear Doppler effect refers to the apparent shift in neutron energy due to relative motion of the neutron and an absorber nucleus. Absorption cross sections of some heavy nuclei have very high, narrow peaks (resonances) at certain energies. Thermal motion of the absorber nuclei will change the capture probability of neutrons near resonance energies in the

following way. Consider a neutron having too low an energy to be captured in a resonance of an absorber nucleus at rest. If thermal motion causes an absorber nucleus to move toward it fast enough, the increased energy corresponding to the increased relative neutron-nucleus velocity will lie within the resonance, and the chance of capture will be much higher. Conversely, neutrons within a resonance can be shifted out of it. For a very dilute concentration of absorber nuclei in a given neutron flux, no net change in absorption with temperature would occur, because as many neutrons would be shifted out of a particulary resonance as into it. If the absorber nuclei are concentrated in a lump, however, as in a reactor fuel element, this compensation will no longer occur. A neutron entering the lump must pass near many absorber nuclei before escaping. For a cold lump, therefore, a neutron with just the right energy has practically no chance of escaping capture, but with energy just outside the resonance will almost certainly escape. If the lump is heated, a slightly off-resonance neutron has a very high probability of passing by a nucleus moving with the right velocity for resonance capture, and a resonance neutron still has a high probability of encountering an absorber nucleus with zero relative velocity, hence of being captured. Thus, the total resonance capture in the lump is increased when the lump is heated. *

For a neutron spectrum of the form ϕ_o/E in the absence of the lump, the effective resonance integral, I, of a lump is defined so that $\phi_o I$ is equal to the total resonance absorption in the lump. The Doppler coefficient is essentially the temperature coefficient of I. Measuring this coefficient thus involves determining a rather small change in I, typically of the order of a few percent for a temperature increase of 1000°K.

Much previous theoretical and experimental work on the Doppler effect in thermal and fast reactors has been discussed by Pearce[1] and Nordheim[2] in comprehensive review articles. The temperature dependence of the Doppler

*The Doppler effect also exists in homogeneous reactors; the previous arguments apply if we read "reactor" for "lump" and recognize that being moderated into or out of the vicinity of the resonance energy is equivalent to entering or leaving the lump.

coefficient is a particularly important subject for investigation, because it drastically affects the total energy release in a reactor excursion. In a 1/E spectrum, calculations usually indicate an approximately $T^{-1/2}$ dependence of the Doppler coefficient, where T is the absolute temperature.[3] (This implies a $\sqrt{T}$ behavior for the resonance absorption itself.) Early Doppler measurements were over too small a temperature range to verify this calculated result. Some later measurements extended the upper temperature limit to 1350°K but were not accurate enough to determine the temperature dependence of the Doppler effect. The results of Hellstrand et al for uranium metal and oxide, measured up to about 1000°K, were consistent with the suggested $\sqrt{T}$ dependence of resonance absorption, although not accurate enough to distinguish between $\sqrt{T}$ and T dependence[4].

The purpose of the investigation described in this report was to measure, in a 1/E spectrum, Doppler coefficients and effective resonance integrals of samples of natural and isotopically enriched tungsten, to as high a temperature as possible. Tungsten is of interest for two reasons. First, it is a logical structural material in high-temperature reactors; in particular, its strength and high melting point make it attractive as a fuel-bearing material,[5] where its Doppler coefficient would play the same role as that of fertile materials in reactors with natural or slightly enriched fuel. Second, the combination of well-known resonance parameters and known spectrum (1/E) make it inherently interesting as a test for current methods of calculating effective resonance integrals and Doppler coefficients. The following points are of interest in this regard:

1) The $\sqrt{T}$ law can be tested to very high temperatures, in principle, because of the refractory properties of tungsten.

2) Natural tungsten consists almost entirely of four isotopes, of masses 182, 183, 184, and 186. Both natural-tungsten samples and samples enriched to more than 93% in W^{182}, W^{184}, and W^{186} were available. Thus, the quantities I and dI/dT could be measured with four different degrees of dilution for each isotope, one for each sample.

3) Significant resonance overlap is possible between some resonance pairs in different isotopes in the natural-tungsten sample; the likeliest possibility is overlap between the 18.8-ev resonance in W^{186} and the 21.1-ev resonance in W^{182}.

4) No correction will be required for fast or epithermal fission in the samples.

The reactivity method was the one chosen for the I and dI/dT measurements, because only one isotope, W^{186}, is amenable to activation measurements. Sample reactivities were measured in a cadmium sleeve at the center of the Sodium Graphite Reactor Critical Assembly (SGR-CA). Extensive calculations of the spectrum at this position as a function of lattice spacing had previously been done for a related program at this laboratory, sponsored by the Atomic Energy Commission, to measure Doppler coefficients of fertile and fissile materials in a 1/E spectrum. Results of these calculations established that the 10.6-in lattice spacing produced the most nearly 1/E spectrum, so that spectral corrections required would be minor[6].

Measured reactivities were converted to resonance integrals in barns by comparison with measured reactivities of gold samples with known resonance integrals. Auxiliary measurements were carried out to assess possible corrections to the experiments, particularly sample scattering effects.

Calculational techniques developed and used at this laboratory were employed to compute effective resonance integrals and Doppler coefficients for the samples measured. Comparison of these results with the measurements served to test the calculational methods. Certain experimental corrections were also calculated, the most important being the correction for deviation of the flux spectrum from 1/E and of the importance spectrum from energy independence.

Nearly all of the major objectives of the program were achieved. Accurate measurements of the sample Doppler coefficients were performed at temperatures up to 1370°K for the natural-tungsten, W^{182}, and W^{186} samples, and up to 1000°K for the W^{184} sample. Proven ovens, previously developed and used in the AEC-sponsored Fast Doppler Measurements program at this laboratory, were utilized for these measurements[7]. Good accuracy was

possible because of the approximately null temperature coefficient of reactivity of these ovens; the temperature limitation was primarily due to the high-temperature decrease in resistivity of the ceramic insulating material used. Doppler measurements up to 2000°K on natural tungsten and 2273°K on W^{184} were made with newly designed ovens containing essentially no ceramic. These ovens were more difficult to use, and turned out to have a large temperature coefficient of reactivity that greatly reduced the accuracy of the measurements. However, the temperature of 2273°K does represent the highest temperature achieved in a critical assembly, to the best of our knowledge, and further development of these ovens and experimental techniques should improve the accuracy of future measurements.

The accuracy of the measurements up to 1370°K is sufficient, and the temperature range large enough, to confirm the $\sqrt{T}$ temperature dependence of the Doppler coefficient predicted by calculations.

Calculated effective resonance integrals were consistently larger than measured ones. For the natural-tungsten sample, resonance overlap can account for nearly all of the difference. In the case of W^{182} and W^{186}, the discrepancies are of the order of 25%, probably indicating the breakdown of one or more of the assumptions made in the calculational method.

Some measurements on the W^{186} Doppler effect using the activation technique were supported by this program. Most of the activation work was performed for the AEC-sponsored 1/E Doppler project, however, and the results will be reported separately.

The remainder of this report is divided into five major sections, followed by two appendices. Section II, "Apparatus and Techniques," is a description of the apparatus used in the experiment, including the critical assembly and the samples, and the techniques employed, such as the method of measuring reactivities. Measurements of effective resonance integrals, including those of samples used to normalize the tungsten results, are discussed in Section III. Results of Doppler-coefficient measurements are presented and analyzed in Section IV, "Elevated-Temperature Measurements." Calculational methods are described and results are compared with experiment in Section V, and Section VI consists of the conclusions.

Appendix A is a description of calculated corrections to the experimental results. Two codes used extensively in analyzing the data are described in Appendix B.

II. APPARATUS AND TECHNIQUES

Measurements of sample reactivities were carried out in a cadmium sleeve at the center of the Sodium Graphite Reactor Critical Assembly (SGR-CA), where the energy dependence of the neutron spectrum is essentially 1/E. Samples were alternately inserted and withdrawn from the core by a mechanical oscillator while the reactor power history was stored in a multichannel analyzer operating in the time mode; the net reactivity difference between the sample-in and sample-out conditions was then determined by numerical solution of the reactor-kinetic equations. Each reactivity measurement was 800 sec long and consisted of four or five complete oscillation cycles. The typical sensitivity of such a measurement was about 0.0015 cents for sample reactivities of a few cents.

To determine Doppler coefficients, reactivity measurements were made at elevated temperatures on tungsten samples heated electrically in small evacuated ovens inside the oscillator tube. The reactivities of heated empty ovens were also measured. For temperatures up to about 1400°K, ovens 0.75 in. OD by 6 in. long, with some ceramic insulation, were used. For higher temperatures (2273°K maximum), ovens 2 in. OD by 13 in. long, essentially all-metal in construction, were used.

Descriptions of the critical assembly, oscillator, ovens, and samples are presented in this section, together with a discussion of the techniques used in making the measurements and analyzing the results.

A. CRITICAL ASSEMBLY

All measurements were made in the Sodium Graphite Reactor Critical Assembly with fuel elements on a triangular 10.6-in. lattice spacing. The assembly consists of a vertical, two-layer array of hexagonal graphite logs, some of which have central holes accommodating fuel elements. Sectional and perspective views are presented in Figures 1 and 2.

Graphite logs are 4 ft high and 4 in. across the flats of the hexagon. Fuel elements used in this project consist of eight hollow cylinders of 1.96-wt-%

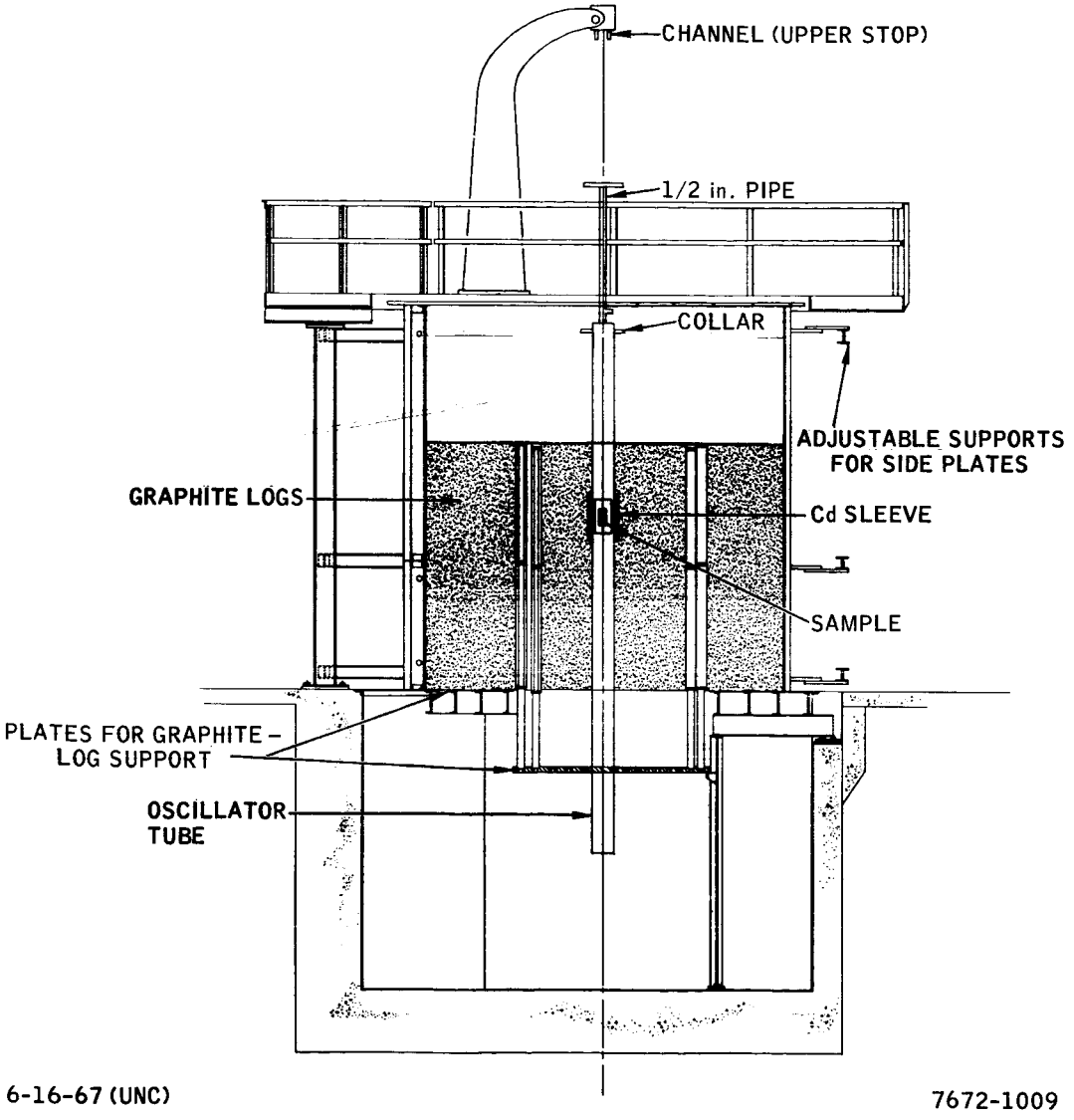

Figure 1. Sectional View of SGR Critical Assembly

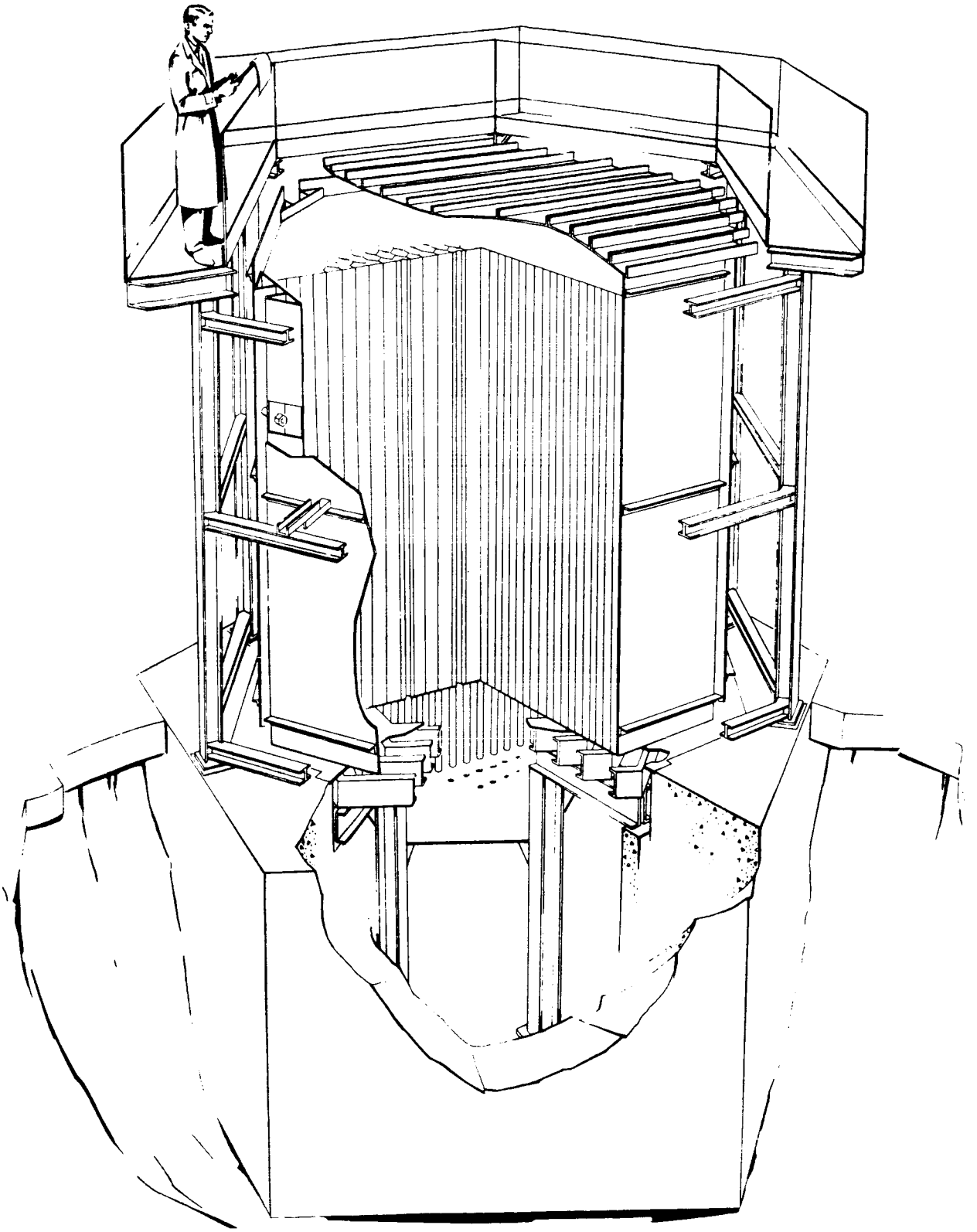

Figure 2. Perspective View of SGR Critical Assembly (Oscillator not shown)

enriched uranium metal stacked in an aluminum tube, 1.875 in. OD and 1.795 in. ID, with no sodium present. Control rods are Y-shaped pieces of silver-cadmium alloy with 0.032-in.-thick blades. A more detailed description of the SGR-CA has appeared elsewhere.[8]

During measurements, samples were located at the geometrical center of the SGR-CA core. A central region of graphite approximately 20 in. in diameter was created by replacing the fuel element normally located at the center with a graphite log. A full-length axial hole, 1-1/4 in. in diameter, was drilled at the center of this log for experimentation. This configuration was chosen because calculations carried out for the parallel AEC-sponsored Doppler Measurements Project indicated that the closest approach to a 1/E spectrum would be obtained at the center of a core having a 10.6-in. lattice spacing with the central fuel element removed.[6] The large central graphite region acts to decouple the sample from the fuel, by flattening the dips in the spectrum at the U^{238} resonance energies and by substantially reducing the fast flux at the sample, thereby minimizing undesired moderation effects due to inelastic scattering in the sample.

This lattice configuration is shown in Figure 3. The core was 8 ft high, axially unreflected, and slightly over 4 ft in diameter with a radial reflector nearly 4 ft thick. For criticality without cadmium in the central hole, 18 fully loaded (8 one-ft-high slugs per element) and three partially loaded (two centered slugs, 3 ft of graphite) elements were required; the latter were the three outermost elements (see Figure 3). Under these conditions, the six central control rods were fully withdrawn, control being maintained with the partially inserted seventh rod at the inner edge of the reflector. Control-rod perturbations on the flux shape and spectrum at the center were thus negligible. Additional fuel loading required for operation with a cadmium sleeve at the center of the central hole was added at the periphery in a symmetrical manner.

Most reactivity measurements were made with a small or large cylindrical cadmium sleeve at the center of the core to exclude thermal neutrons from the sample. Both sleeves had a wall thickness of 0.031 in. The smaller sleeve, 1.27 in. ID by 6 in. high, was used for room-temperature measurements and

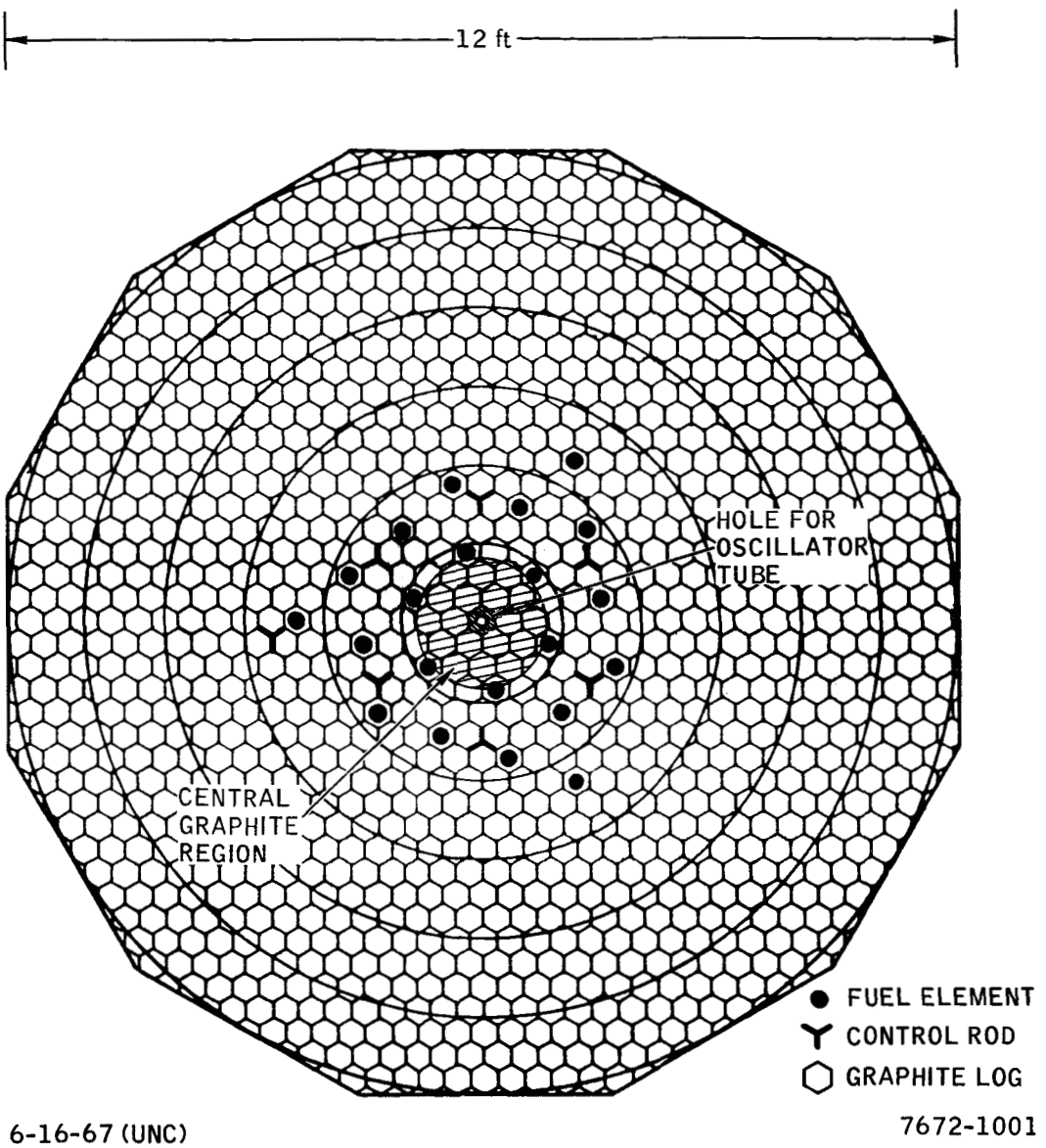

Figure 3. SGR-CA Critical Core Loading for 10.6-in. Lattice Spacing

(Sample is inserted into full-height axial hole at center of core. Cross hatching denotes central graphite region providing 1/E spectrum in axial hole. All control rods are withdrawn during measurement except one at far left.)

elevated-temperature measurements up to 1400°K. The diameter of the 1.25-in. axial hole in the central graphite log was enlarged to 1.33 in. over a height of 6 in. at the vertical center of the log to provide a recessed space to hold the sleeve. The critical loading with this sleeve in place was 20.6 fuel elements (compared with 19.4 elements without the sleeve).

The larger oven used for measurements above 1400°K required a larger cadmium sleeve, 2.723 in. ID by 18 in. high. A new central graphite log was used with a 2.687-in.-diam center hole. The diameter of the central 18 in. of the hole was enlarged to 2.81 in. to take the sleeve, which was completely encased in a stainless-steel jacket, 0.004-in. wall thickness, for containment. This sleeve necessitated an increase in fuel loading to 25.6 elements.

Measurements made without cadmium were performed in the 1.33-in.-diam cavity used for the smaller sleeve.

B. DETERMINATION OF REACTIVITY

The reactivity change due to insertion of the sample in the central axial hole was determined by means of the "dynamic reactivity" technique. In this method, the power history of the reactor is recorded on a multichannel time analyzer while the sample is alternately inserted and withdrawn by a mechanical oscillator. The number of counts recorded in each channel then serves as input to a computer code that solves the reactor-kinetic equations numerically to determine the reactivity at each time step.

1. Oscillator Description

The mechanical oscillator used to insert and remove the sample consisted of a cable-and-drum unit driven by a reversible motor, a small crane, and a 13-ft aluminum tube, 1.25 in. OD. The crane rested on the steel floor above the reactor with the pulley at the end of its arm directly above the central hole in the core. The 13-ft tube was always fully inserted in the hole; at its top, it was attached to a cable that passed through the pulley to the drive unit. The reversible motor was controlled by a dual-preset scaler driven by a crystal-controlled oscillator.

The center of the sample being measured was located 27 in. above the vertical center of the 13-ft oscillator tube. For most measurements an additional sample holder ("dummy") centered 27 in. below the center of the oscillator tube was also used. Thus, with the oscillator tube at the top of its 54-in. stroke, the dummy position was at the center of the 96-in.-high core, the sample position was 6 in. above the top of the core, and the bottom of the oscillator tube was 3 in. below the bottom of the core. With the oscillator tube at the bottom of its stroke, the sample position was at the core center, and the dummy position was 6 in. below the bottom of the reactor. A mechanical stop at each end of the stroke positioned both sample and dummy in a precise, reproducible way, and simultaneous activation of a microswitch shut off the drive unit.

2. Procedure

A compensated ionization chamber located in the radial reflector (2 ft above the core midplane, at a radius of 5 ft) was used to provide a signal proportional to reactor power. This signal fed a voltage-to-frequency converter connected to a 400-channel analyzer in the multiscaler (time) mode. The number of counts in each channel was thus proportional to the time-integrated power over the channel width (usually 2 sec).

To make a reactivity measurement, the reactor was made critical with the oscillator tube at the top of its travel (sample out). Level power was maintained for about ten minutes to ensure that the initial reactivity was approximately zero with delayed-neutron precursors at their equilibrium values. The analyzer and oscillator timer were then started simultaneously. After 70 sec at level power, the oscillator tube was driven all the way in. The sample remained at the core center for 60 sec; the tube was then returned to its original position, where it remained for another 60 sec, to remeasure the base-point reactivity. Transit time was about 20 sec in either direction. This 160-sec cycle was repeated 4-1/2 times during each 800-sec measurement. Use of an odd number (7 or 9) of half-cycles permitted more convenient mathematical elimination of linear drift from the measurements.

3. Dynamic-Reactivity Code

Reactivity as a function of time was calculated from the analyzer data by a computer code. For use in this code, the reactor-kinetic equations have been transformed into one integrodifferential equation in which reactivity is the unknown quantity and reactor neutron population (or any quantity proportional to it, such as the ion-chamber signal for this experiment) appears in a sum of integrals over known variables.[9]

This computer code was originally used mainly for control-rod calibrations; modifications were necessary to make it more useful for precise measurement of small reactivities. The two most important modifications were a feature to compute a number of weighted-average reactivity values from the individual reactivities and the use of an exponential approximation for the variation of power over a single channel. The averaging procedure is carried out in such a way that long-term linear drift is cancelled out. The code (RHOAV) is described in somewhat more detail in Appendix B.

Only reactivity values corresponding to times when the sample was stationary in the in or out positions were used to determine the reactivity difference between sample-in and sample-out positions. The reactivities measured were small enough that the spatial distribution of the delayed-neutron precursors remained essentially undisturbed in the fundamental mode, so that the assumption of space-time separability implicit in the usual form of the reactor-kinetic equations was valid. (For very large reactivity changes, such as result from rod drops, departure of the precursors from the fundamental mode can be observed as a gradual drift of the calculated values away from a previously established constant value. No such drift has been observed in these experiments. Results are also independent of detector location.)

The main source of error in this technique is the random fluctuations of the neutron population of the reactor, as sampled by the detector; therefore, the uncertainty of a given measurement is inversely proportional to the square root of the product of power level and measurement time. In the SGR-CA operating at full power, typical results of reactivity measurements lasting 800 sec (of which 540 sec represented useful measurement time) had standard

deviations of the order of 0.0015¢. This value agrees with the expected value for reactor noise calculated from average power, oscillation frequency, detector efficiency, and reactor transfer function.

The dynamic method of measuring sample reactivities offers some advantages over other commonly used methods. As used in these experiments it requires a mechanical oscillator, but this oscillator can be much simpler in construction and operation than most pile oscillators. No attempt is made to produce sinusoidal reactivity changes, as is sometimes done. Neither is it necessary to have a rapid transit time (that is, to fire the sample in or out in a fraction of a second) to avoid introducing undesired power transients into the Fourier analysis. Only those portions of reactivity data taken while the sample is at rest are used, so that the relatively long transit times due to the simple cable-and-drum mechanism are acceptable.

The dynamic method requires less measurement time than the period method for equivalent accuracy, because of the elimination of the long waiting time required for complete decay of the initial transient.[10] The waiting time would be prohibitive for most of the reactivities measured in this program, which were of the order of two cents. This elimination of waiting time also allows frequent remeasurement of the reactivity of the critical assembly with the sample out (the zero-point reactivity), to eliminate the effects of long-term drift.

C. ROOM-TEMPERATURE MEASUREMENTS

For measurements of sample reactivities at room temperature, the small oscillator tube (1.25-in. OD) was filled with graphite except for two cylindrical cavities, one at the sample position and one at the dummy position. These cavities were normally 0.44 in. in diameter and 4 in. long to accommodate standard-size samples, which were 0.438 in. in diameter and 4.0 in. long. At the sample position, the oscillator tube could be opened to provide access to a 6-in.-long cavity with diameter equal to the full 1.15-in. ID of the tube; this cavity could then be filled with graphite pieces of various sizes to accommodate samples of either standard or nonstandard dimensions.

Since total sample worths were being measured, rather than changes in the worth of a particular sample, the dummy position was left empty. Two separate measurements were made to determine each sample worth, one with the sample surrounded by graphite in the sample position and one with the sample (but not the graphite) removed. The difference of these two measurements thus represents the sample reactivity relative to void.

D. ELEVATED-TEMPERATURE MEASUREMENTS

1. Apparatus

a. Measurements Below 1400°K

(1) Oven Description

The ovens used to heat samples to a maximum temperature of about 1400°K were nearly identical to those developed and used by the AEC-sponsored Fast Doppler project.[7] They are characterized by relatively small size, small temperature coefficient of reactivity, and low power requirements (e.g., 25 watts for 1000°K, 100 watts for 1370°K).

A typical oven consists of an insulating core that surrounds the sample, made of a machinable ceramic (lavite, primarily aluminum silicate); a nichrome heating element wound on the core; a lavite sleeve over the heating element; a molybdenum heat shield around the sleeve; expansion washers and insulators at the ends; and a stainless-steel shell. The inner diameter of the heater system is 0.448 in., and it normally accepts samples 4 in. long. The shell is 0.75 in. OD by 5 in. long. Sample temperatures are measured with two stainless-steel-sheathed, MgO-insulated chromel-alumel thermocouples, one in a central axial hole 1.5 in. deep and one in a 1/4-in.-deep hole at a radius of 1/8 in. Oven components are shown in Figure 4.

Before each run, the system is evacuated and baked out for about 20 hr at a temperature slightly higher than the highest anticipated experimental temperature. The sample is then allowed to cool, and the system is sealed

by crimping off a copper evacuation tube. Reheating the closed system through many temperature cycles over a period of several weeks normally does not degrade the vacuum significantly.

(2) Oscillator Tube

A second oscillator tube was assembled for use in elevated-temperature measurements up to 1400°K. It was similar to the one described in sections IIB1 and IIC except that it contained no graphite, to allow unimpeded passage of cooling air. Provision was also made for the exit of thermocouple and heater wires. Two rods, symmetrically located 24-3/8 in. above and below the center of the tube, were welded across the interior of the tube to act as mechanical stops for the sample and dummy ovens. Several extra ovens and hardware for mounting them inside the oscillator tube were fabricated.

b. Measurements Extending Above 1400°K

The achievement of sample temperatures in the 2000°K range required an oven that was physically much larger and more massive than the lower-temperature ovens. The increased size of this oven led directly to new requirements for the oscillator tube and cadmium sleeve.

(1) Oven Description

Initial attempts to develop a 2000°C oven similar in design to the ovens used below 1400°K, with high-temperature ceramic insulating materials (alumina, zirconia, thoria) used in place of lavite, proved unsuccessful. After an improvement of only two or three hundred degrees over the lavite ovens, the insulators became electrically conductive enough that electrical shorting between turns of the heater coil took place. Attention was then turned to an all-metal design that depended solely on a high vacuum for electrical insulation of the heating coil. This design proved to be successful in achieving sample temperatures above 2000°K.

The main elements of this oven are shown in Figure 5.

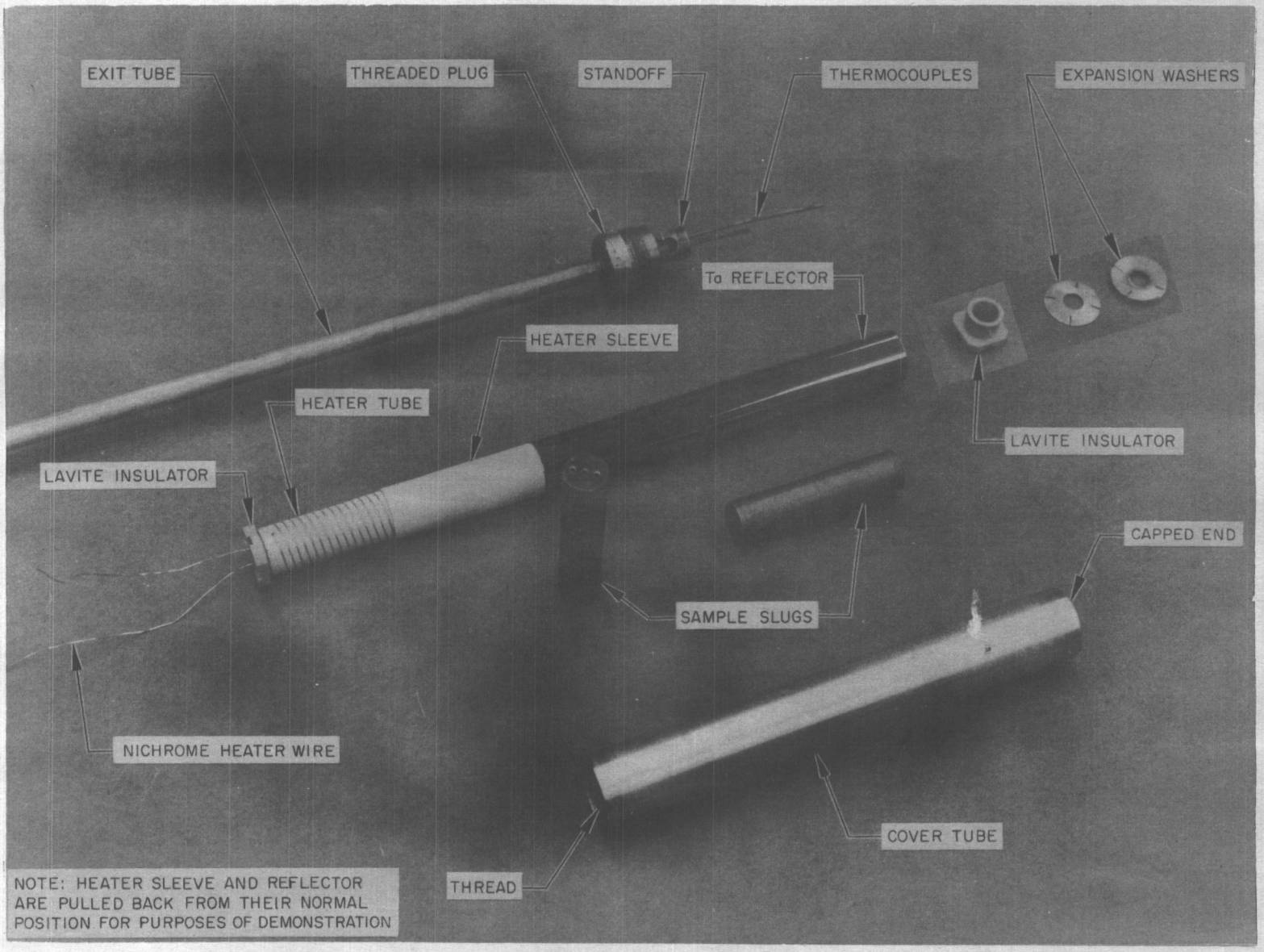

Figure 4. Disassembled 1400°K Oven

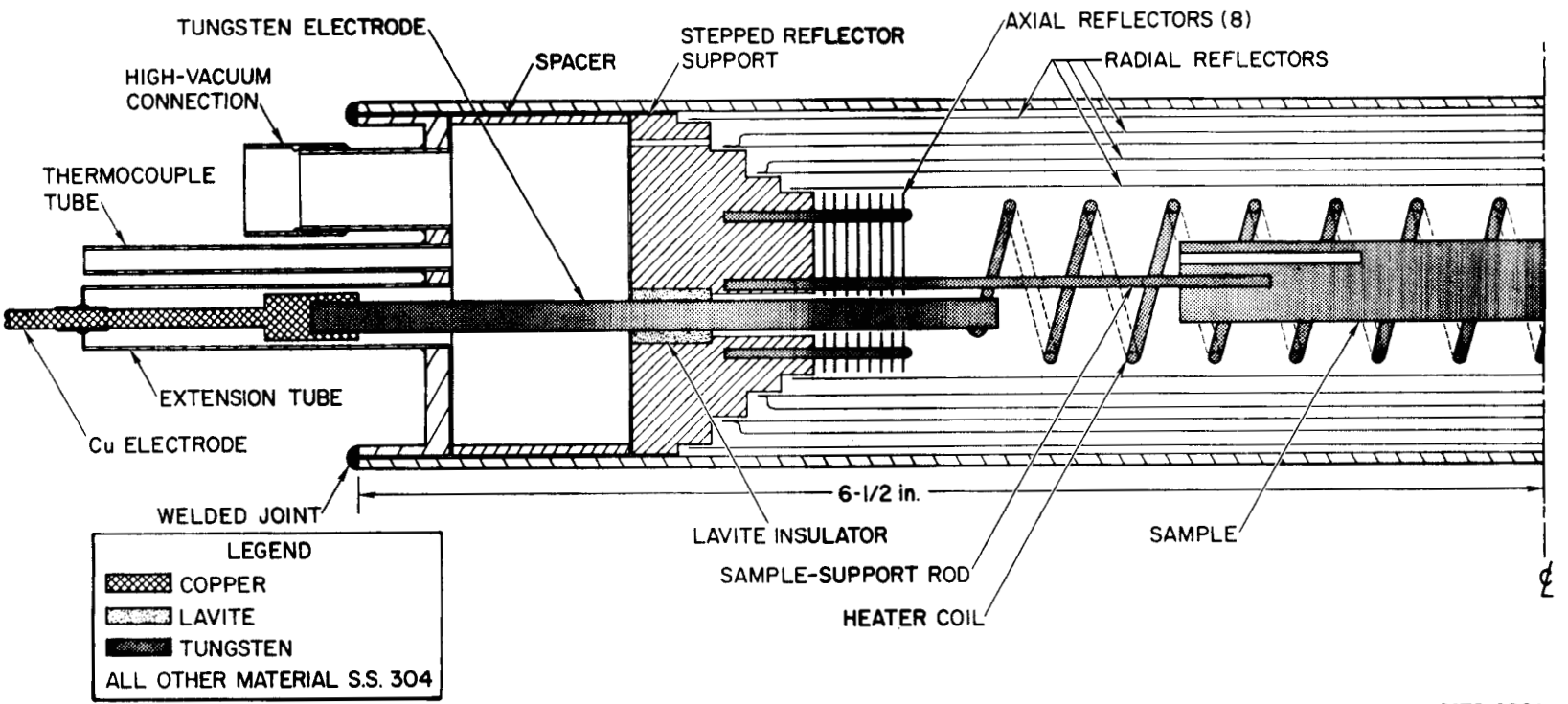

Figure 5. Partial Sectional View of 2000°C Oven
(Not shown: Thermocouples in sample and stepped reflector support, thermocouple leads, most pumpout holes in stepped reflector support, axial-reflector spacers, alignment posts in end cap. Other half of oven is identical with half shown, except for lack of high-vacuum connection and thermocouple tube in end.)

The sample was supported by two 1/16-in.-diam tungsten rods, 3 in. long, embedded in each end to a depth of 1/2 in. along the axis. The other ends of these rods were inserted 1/2 in. into the two stainless-steel reflector supports.

Heat was supplied to the sample by thermal radiation from a free-standing, current-carrying coil of 1/16-in.-diam tungsten wire surrounding the sample. The diameter of the coil was 7/8 in., with a total of 14 turns in its overall length of 5 in. The coil thus extended 1/2 in. beyond each end of the sample, to provide a more uniform axial temperature distribution in the sample. The ends of the coil were attached to two 5/32-in.-diam, 7-in.-long tungsten electrodes that supported the coil and supplied the current required to heat the sample. Each electrode passed through holes in the axial reflectors, reflector support, and end cap into an extension tube attached to the end cap, where connection was made to the external power source.

Heat losses from the coil and sample were reduced by radial and axial molybdenum reflectors. The four outer radial reflectors were 0.001 in. thick; all other radial reflectors were 0.005 in. thick.

Because of clearance required between sample, coil and the numerous radial reflectors, principally to minimize the effects of component thermal expansion and coil sagging, the physical size of the new systems was substantially larger than that of the previously used ovens. The outer diameter of the shell was 2 in., the overall length 13 in.

An external vacuum system, consisting of a forepump, sorption pump, and diffusion pump, was used to keep the residual pressure in the oven below 10^{-3} torr during operation. There were no gaskets in the oven; after assembly, the vacuum seal between shell and end caps was made by welding.

Power requirements were modest at low sample temperatures but increased sharply as 2300°K was approached. For example, although 1000°K was achieved with only 25 watts and 1500°K with 110 watts, a power level of 600 watts was needed to reach 2000°K, and 2273°K required 2200 watts. Continued development of this oven for related AEC-sponsored projects has not, as yet, resulted in significant improvement in the high power requirements at high temperatures.

Sample temperatures were measured with a single tungsten-rhenium (W-5Re/W-26Re or W/W-26Re) thermocouple, magnesia insulated and tantalum sheathed. The thermocouple was fully inserted in a longtiudinal hole in each sample, 0.062 in. diameter and 1 in. deep, with the axis of the hole 1/8 in. from the axis of the sample.

(2) Oscillator Tube

The first requirement inposed by the larger ovens was a larger-diameter oscillator tube. The new tube, also made of aluminum, was 2-5/8 in. in OD, 0.065 in. in wall thickness, and 14 ft long. Thermocouple leads, the high vacuum and compressed-air lines, and one heater cable were brought out through the top; the other heater lead was brought out through the bottom of the tube, which was always below the bottom of the core.

The additional mass of steel in the large ovens caused them to have much higher thermal-neutron worths than the previously used ovens. The rapid disappearance of this large thermal reactivity as the oven moved into the cadmium sleeve could have led to a momentarily large reactivity-insertion rate, possibly exceeding for a short time the maximum rate allowed by the operating rules. To circumvent this problem, a reactivity-shimming technique was used. The thermal reactivity of an empty oven was first measured; then reactivities of 13-in. lengths of various types of tubing on hand were measured. It was found that the nested combination of 2-1/8-in.-OD, 0.070-in.-wall copper tubing and 1-3/4-in.-OD, 0.65-in.-wall stainless-steel tubing had about the same thermal-neutron worth as the oven. Two pairs of concentric tubes of the above dimensions were then added to the oscillator tube, one pair extending from the top of the oven to the top plug of the tube, the other from the bottom of the oven to the bottom plug. The oscillator tube thus presented an approximately constant thermal reactivity worth per unit length to the reactor as it was moved through the core. The reactivity-insertion rate was greatly reduced by this modification, and was reduced still more by the substitution of a smaller gear in the drive unit, a change needed to overcome the much greater weight of the large oscillator tube.

As before, the fully in and fully out positions of the oscillator were established by mechanical limits, and microswitches were also provided to shut off the drive motor at both ends of the stroke.

2. Procedure

Measurements of reactivities at elevated temperatures were performed with a sample in the heated oven and a similar sample (it need not be identical) in the cold, dummy oven. The only purpose of making the dummy system similar to the sample system is to reduce the magnitude of the power swings; the reactivity code is then more accurate. The reactivity difference of interest is that between the sample at two different temperatures, not that between sample and dummy. The magnitude of oven reactivity effects was determined by separate reactivity measurements on a heated empty oven.

Several runs were made with each sample, one run normally taking one day using the small ovens. Data from each run, consisting of a set of power measurements at each of several sample temperatures, were analyzed first with the RHOAV code (Appendix A) to determine the sample reactivity at each temperature. These reactivities were then analyzed to determine the best-fitting form of the temperature dependence of the Doppler effect with the DOPFIT code (Appendix B).

Results of analysis of a typical run are shown in Figure 6, an example of DOPFIT graphical output. Errors shown on the individual reactivities were the statistical errors computed by RHOAV. The curve is a weighted least squares fit to the reactivity-vs-temperature data, having the form

$$\rho = a + b\, T^{1-\gamma}, \qquad \ldots (1)$$

where γ is varied in steps of 0.1 from 0 to 1.5 to find the value producing the best fit. The Doppler coefficient then has the form $d\rho/dT = b(1-\gamma)\, T^{-\gamma}$. In this run, the value of γ leading to the best fit was 1/2.

The procedure for taking data with the large ovens was essentially the same. Fewer points were measured at the lower temperatures because the coverage of the small-oven measurements was believed to be adequate there. At the higher temperatures (above 1400°K), the sample temperature reached equilibrium within 15 min after increasing power, but temperatures of other

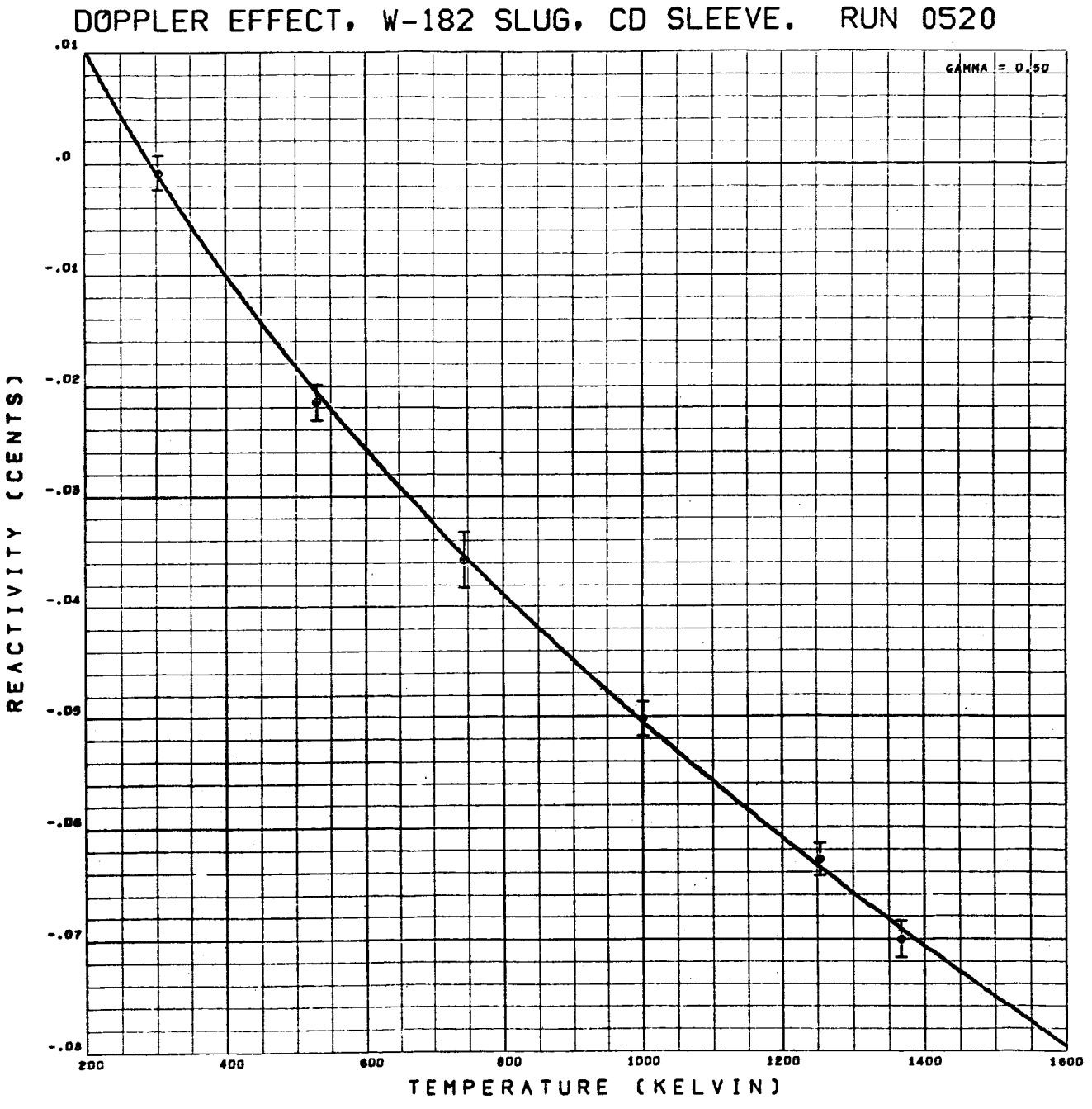

Figure 6. Experimental Points and Least-squares Fit for Doppler Measurements on W^{182}, Single Run.

parts of the oven continued to rise. The long thermal time constant of this oven made any attempt to wait for thermal equilibrium of all oven components impractical.

No dummy oven was necessary, since the reactivity-shimming technique minimized the power variation between in and out positions.

A number of difficulties prevented carrying out an extensive series of measurements in the 2000°K range before conclusion of the project. The initial measurements were terminated by pressure increases in the oven, from various causes, at temperatures above 1900°K. After each run terminated in this way, it was necessary to disassemble the oven, clean the steel parts chemically, and fabricate a new heater coil and new reflectors, before reuse of the oven. These problems were gradually overcome, and did not recur during the final run, W^{184} at 2273°K. Even without these difficulties, the length of time involved in assembly and disassembly of the oscillator tube and reactivity shims, welding shut or filing open the oven, and in completely dismantling and reassembling the oven for each run (necessary because of the manner of its construction) was considerable, so that only a few high-temperature runs could be made in the time remaining.

E. SAMPLE PROPERTIES

Relevant properties of the tungsten samples used in this experiment are presented in Table 1. Properties of gold samples, used to normalize reactivity measurements, are given in Table 2, and those of samples used in auxiliary measurements are listed in Table 3.

TABLE 1

PROPERTIES OF TUNGSTEN SAMPLES

Principal Isotope in Sample	M (gm)	M/A (moles)	Diameter (in.)	Length (in.)	$\sqrt{S/M}$* (cm/gm$^{1/2}$)	s* (barns)	Isotopic Composition† (at. %)			
							182	183	184	186
Natural	61.58	0.3349	0.2495	3.997	0.5818	25.83	26.34	14.30	30.68	28.68
Natural	179.38	0.9757	0.4380	4.000	0.4569	15.94				
Natural	184.43	1.0032	0.4387	3.962	0.4490	15.39				
Natural	188.46	1.0251	0.4365	4.000	0.4458	15.11				
182	183.20	1.0060	0.4375	4.000	0.4519	15.44	93.43	2.67	2.57	1.32
184	176.76	0.9609	0.4378	4.001	0.4602	16.17	1.54	1.59	94.40	2.47
186	188.67	1.0151	0.4385	4.000	0.4459	15.43	0.70	0.63	1.53	97.14

*To determine effective S/M or s for individual isotopes in sample, divide value in table by atom fraction of isotope.

† W^{180} has been neglected in natural tungsten; other atom fractions were renormalized accordingly. W^{180} atom fraction in enriched samples was less than 0.05%.

Nomenclature: M = mass; A = mean sample atomic weight; S = surface area (including ends); s = geometrical escape cross section = S/4NV $= \frac{A}{4N_o}\frac{S}{M}$, where N is atom density, V is volume, and N_o is Avogadro's number

TABLE 2

PROPERTIES OF GOLD SAMPLES

M (gm)	M/A (moles)	Diameter or Thickness* (in.)	Width* (in.)	Length (in.)	$\sqrt{S/M}$ (cm/gm$^{1/2}$)	s (barns)
2.683	0.01362	0.002*	1.045	4.00	4.489	1649.
0.876	0.004445	0.030	-	4.00	1.669	227.9
38.09	0.1933	0.031*	0.990	4.00	1.179	113.8
49.87	0.2532	0.235	-	3.683	0.6024	29.68
74.4	0.3777	0.670	-	0.670	0.4284	15.00
148.8	0.7553	0.670	-	1.340	0.3910	12.50
223.2	1.133	0.670	-	2.010	0.3778	11.66
297.4	1.510	0.670	-	2.680	0.3711	11.25

(See Table 1 for definitions of symbols.)

*Rectangular sample

TABLE 3

PROPERTIES OF MISCELLANEOUS SAMPLES

Material	M (gm)	M/A (moles)	$\sqrt{S/M}$ (cm/gm$^{1/2}$)	s (barns)
Lead	110.6	0.533	0.582	29.2
Stainless Steel	77.9	1.394	0.693	11.15
Aluminum	28.7	1.065	1.142	14.60
Lavite	23.3	0.055	1.268	284.

All samples were 0.438 in. diam by 4.00 in. long.

III. MEASUREMENTS OF EFFECTIVE RESONANCE INTEGRALS

A. CALIBRATION

If the spectra of both neutron flux and importance are lethargy independent, the measured reactivity of a sample under cadmium will be proportional to its effective resonance integral. The constant of proportionality, C, cannot be calculated a priori with reasonable accuracy; it must be determined experimentally by measuring the reactivity of one or more samples with known resonance integrals. In this experiment, gold was chosen as the reference standard. Beller and Farrar have recently reported results of measurements of the effective resonance integrals of plane gold samples over a wide range of surface-to-mass ratio.[6] The reactivities of two plane samples, 0.002 and 0.031 in. thick, were measured in the SGR-CA, and their resonance integrals were determined from a plot of Beller and Farrar's measurements. Their results are given as effective resonance integrals vs $\underline{s}$, the geometrical escape cross section for a lump.* For the range of the two samples used, the effective resonance integral I is proportional to $\sqrt{s}$.

The effective cadmium cutoff energy for Beller and Farrar's samples should be approximately equal to that for reactivity measurements in the 0.031-in. cadmium sleeve, since their activation measurements were performed in a 0.062-in.-thick cadmium box.

The calibration constant C is defined as

$$C = \frac{I_s}{\rho_s} = \frac{I_s}{f_s \rho_{ms}}, \qquad (2)$$

*The quantity $\underline{s}$ can be thought of as a geometrical cross section for escaping capture in a lump; it is defined as $\underline{s} = S/4NV = 1/N\ell$, where ℓ (=4V/S) is the mean chord length of the lump. (The other quantities were defined in Table 1.) The utility of $\underline{s}$ is the fact that it can be used to extend homogeneous resonance-integral calculations to heterogeneous systems; $\underline{s}$ plays the role of a scattering cross section in this formulation.

where I_s is the known resonance integral of the standard, ρ_s is the reactivity per mole that the standard would produce in a 1/E spectrum, f_s is the correction factor for a non-1/E spectrum and ρ_{ms} is the measured reactivity per mole of the standard. (See Appendix A for method of calculating $\underline{f}$.)

Results for the calibration constant C are given in Table 4.

TABLE 4

EPICADMIUM CALIBRATION CONSTANT

Gold Sample Thickness* (in.)	$\sqrt{S/M}$ ($cm/gm^{1/2}$)	I† (barns)	Reactivity (¢/mole)	f_s§	C'**	C
					(barn-mole/¢)	
0.002	4.489	425 ± 7	29.71 ± 0.04	1.005	14.29	14.22 ± 0.24
0.031	1.179	132.6 ± 2.0	8.542 ± 0.005	1.109	15.52	14.00 ± 0.24

*From Table 2; see that table for other sample properties.
†Measured by Beller and Farrar.(6)
§f_s is calculated spectral correction factor.
**C' is calibration constant uncorrected for spectral deviation.

It is clear that the spectral corrections bring the two measurements of C into reasonable agreement. (Nearly all of the error quoted for each value is due to uncertainty in the absolute normalization of Beller and Farrar's measurements, so that the two errors are correlated. The agreement is, therefore, not within experimental error.) Since one measurement has a calculated spectral correction of 11%, it must be given less weight. (This is a reflection of the greater sensitivity of thicker samples to the cadmium spectral depression.) Without an extensive experimental or analytical investigation of the validity of calculated spectral corrections, it is difficult to estimate the error in the corrections.* The procedure adopted here is to arbitrarily assign to $\underline{f}$ an error of (f-1)/2. The error in C from this source is negligible for the thinner

* There is some indication that diffusion theory may overestimate this correction. See Appendix A.

sample and amounts to 5.5% for the thicker. With this assignment, the value of C measured with the thicker sample does not contribute to the weighted mean, although consistent with it.

The resultant measured value of epithermal calibration constant is thus $C = 14.22 \pm 0.24$ barn-mole/¢.

Reactivities of a number of cylindrical gold samples were also measured and converted to effective resonance integrals. Data needed to calculate spectral corrections were available only for the sample having $\sqrt{S/M} = 0.6024$, for which the correction factor f was 1.108. This value was almost identical to the correction factor for the thicker plane sample (Table 4). The uncorrected value of C (15.52 barn-moles/¢) determined for that sample was therefore used for all of these relatively thick samples. An additional error of 3% was arbitrarily assigned to these measurements to allow for the lack of additional spectral corrections.

These results are presented in Table 5 and Figure 7. Some of the results of Beller and Farrar are also included in this figure.

TABLE 5

MEASURED EFFECTIVE RESONANCE INTEGRALS OF GOLD CYLINDERS

$\sqrt{S/M}$* ($cm/gm^{1/2}$)	Reactivity (¢/mole)	I† (barns)
1.669	12.49±0.16	194.± 7.
0.6024	4.729± 0.04	73.4± 2.5
0.4284	2.993± 0.003	46.5± 1.6
0.3910	2.624± 0.002	40.7± 1.3
0.3778	2.484± 0.002	38.6± 1.3
0.3711	2.405± 0.002	37.3± 1.3

*See Table 2 for other sample properties.
†Based on C = 15.52 barn-moles/¢ for thick gold samples (Table 4), otherwise uncorrected for spectral deviation.

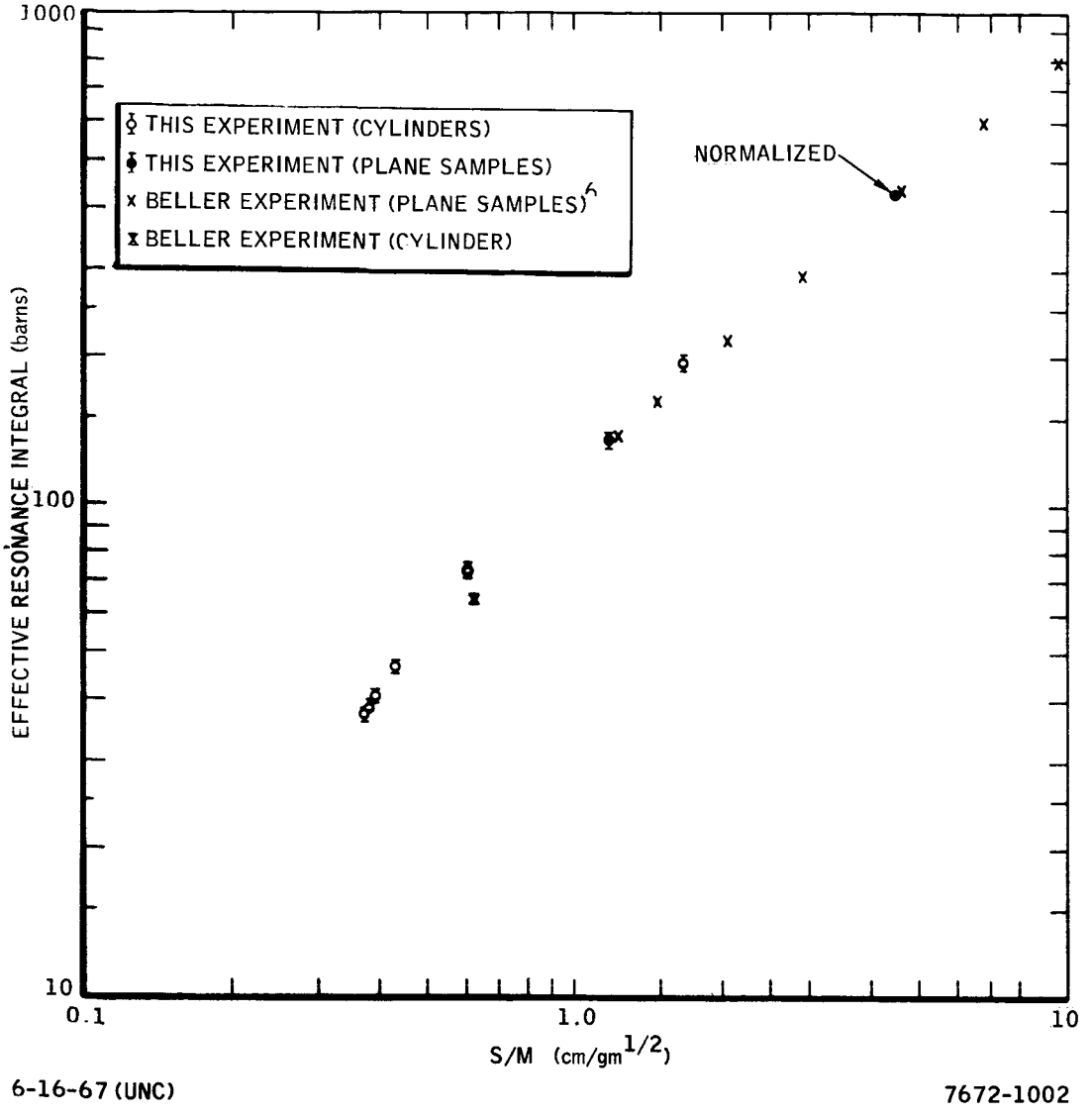

Figure 7. Measurements of Effective Resonance Integral of Gold Samples

B. AUXILIARY MEASUREMENTS

1. Miscellaneous Reactivity Effects

Possible effects of scattering on reactivity were investigated by measuring reactivities of samples of a heavy scatterer, lead, and a light scatterer, aluminum. In particular, lead has a very high ratio of scattering to absorption.

Measurements on samples of stainless steel and lavite served to check the smallness of reactivity effects of the principal structural materials used in the ovens. These samples were in considerably more concentrated form than the materials in the ovens.

Results of reactivity measurements on these four materials are given in Table 6.

TABLE 6
REACTIVITIES OF MISCELLANEOUS SAMPLES

Material	Mass * (gm)	Reactivity (¢/mole)
Lead	110.6	0.009 ± 0.008
Stainless Steel	77.9	-0.131 ± 0.006
Aluminum	28.7	0.000 ± 0.004
Lavite	23.3	-0.75 ± 0.15

(All samples were 0.438 in. diam by 4.0 in. long.)
*See Table 3 for other sample properties.

Scattering effects on sample reactivities were also investigated by determining the effect of surrounding a 0.25-in.-diam natural-tungsten slug with a thick hollow cylinder of lead. Wall thickness of the lead cylinder was 0.092 in. Without the additional cylinder, the measured epicadmium reactivity of the tungsten slug was 2.527±0.016¢/mole; with the external lead cylinder in place, the result was 2.511±0.002¢/mole.

All of the foregoing measurements were made with two cadmium end caps, 1.15 in. diam by 0.031 in. thick, at the ends of the sample in the oscillator tube. These caps were worth only 0.25¢, but more important is the fact that measurements on two standard natural-tungsten samples without end caps agreed, within error, with measurements on the same samples with end caps. In view of the demonstrated smallness of end effects, all subsequent measurements in the sleeve were done without end caps. Possible reactivity errors due to slightly different positions of the end caps between sample and void measurements were thus eliminated, as well as problems involving heating of the caps during measurements at elevated temperatures.

2. Axial Flux and Importance Shapes

Axial traverses in the 2-in.-diam central axial void were made with a fission counter and an Sb-Be neutron source to verify the expected cosine shape for real or adjoint flux. The fission-counter data were fitted quite well (rms deviation less than 0.2%) by a cosine with the expected parameters. If the source traverse is made at two different power levels, the source importance can be separated from the resulting reactivity data.[9] Within the rather large scatter of the experimental points, the source-importance data were also fitted with a cosine (rms deviation about 5%). The maximum variation in the product of flux and importance over the length of a 4-in. sample is 0.4% with the parameters determined from these fits.

C. RESULTS

Four samples of natural tungsten and three of enriched were measured in the cadmium sleeve. Resultant reactivities were then converted into effective resonance integrals in barns with the calibration constant C and calculated spectral-correction factors. The effective cadmium cutoff energy, which is the lower energy limit of the effective resonance integral, was taken to be 0.622 ev* from the tables of Stoughton et al.[11] Results are given in Table 7.

*This energy corresponds to a cadmium thickness of 0.062. in., twice the actual wall thickness, since a reactivity measurement cannot distinguish between a neutron captured in the sample and a neutron that leaves the sample and is then captured in the cadmium sleeve. The effective cadmium thickness for a reactivity measurement is thus twice that for an activation measurement.

TABLE 7

MEASURED EFFECTIVE RESONANCE INTEGRALS
(above 0.622 ev) OF TUNGSTEN SAMPLES

Principal Isotope In Sample	$\sqrt{S/M}$ * ($cm/gm^{1/2}$)	Reactivity (¢/mole)	Spectral Correction Factor †	Effective Resonance Integral§ (barns)
Natural	0.582	2.527±0.016	1.002±0.001	36.0±0.7
Natural	0.457	1.967±0.002	0.996±0.002	27.8±0.5
Natural	0.449	1.930±0.001	0.996±0.002	27.3±0.5
Natural	0.446	1.917±0.001	0.996±0.002	27.2±0.5
182 (93%)	0.452	1.759±0.001	1.044±0.022	26.1±0.7
184 (94%)	0.460	0.724±0.003	0.956±0.022	9.84±0.28
186 (97%)	0.446	1.718±0.001	1.086±0.043	26.5±1.2

*See Table II-1 for other sample properties.
†Error in f is assumed to be (1-f)/2.
§Including 1/v contribution.

D. ERROR ANALYSIS

Quoted uncertainties in the reactivities listed in Tables 5 through 7 were based on statistical analyses of the individual measurements and, for gold and tungsten, reproducibility of repeated measurements. As a rule, reactivity uncertainties did not contribute significantly to the final quoted uncertainties in effective resonance integrals.

Uncertainty in the calibration constant, C, was the principal contributor to quoted errors in the effective resonance integrals for natural-tungsten samples. This uncertainty amounted to 1.7%, arising almost entirely from uncertainty in the infinitely dilute gold resonance integral to which Beller and Farrar's results were normalized.

For the other samples, notably W^{186}, the principal source of error was the assumed uncertainty of (f-1)/2 in the spectral correction factor, $\underline{f}$. This uncertainty assignment does not depend on the normalization of $\underline{f}$, because the uncertainty in correction factor for sample $\underline{x}$ is taken to be the uncertainty in the ratio f_x/f_{Au}, where f_{Au} is the correction factor for the standardizing gold sample.

For a sample at the center of the reactor, internal moderation by the sample can not affect reactivity unless the neutron energy loss caused by collision with a sample nucleus is large enough that the importance of the neutron is significantly different from its value before the collision. This can occur only for inelastic scattering. Other scattering effects on reactivity are proportional to the gradients in flux and importance, which are essentially zero over the sample volume. Inelastic scattering occurs mainly above 0.1 Mev; the flux of neutrons with this energy or higher is greatly reduced by the large moderator region surrounding the sample, so that the inelastic-scattering effect on reactivity should be small. This expectation is borne out by the results of the two auxiliary experiments involving lead. The reactivity of the lead sample was nearly zero, being positive and only slightly larger than the standard deviation of the measurement. In the other lead measurements, the reactivity of the 0.25-in.-diam tungsten sample was unchanged by addition of a surrounding lead cylinder with 0.092-in. wall thickness. Internal moderation in the aluminum sample proved to be completely negligible.

Inleakage of thermal neutrons through the open ends of the cadmium cylinder caused negligible effects on sample reactivity. This was established by the fact that in all cases where samples were measured both with and without cadmium end caps, the resultant reactivities agreed within experimental uncertainties. In addition, solid-angle calculations indicate that the fraction of all incident thermal neutrons that would cause a sample-dependent reactivity signal is approximately 0.04%.

Variation of axial flux and importance over the sample length is also negligible; the average value of their product over the sample length differs by only 0.1% from the value at the center.

To summarize, the major contributors to uncertainty in measured effective resonance integrals are uncertainties in the calibration constant and spectral correction factors.

IV. ELEVATED-TEMPERATURE MEASUREMENTS

A. MEASUREMENTS BELOW 1400°K

1. Results

Sample reactivities as functions of temperature were measured up to approximately 1370°K for natural tungsten, W^{182}, and W^{186}. Repeated runs were made up to 1000°K; then a final run was made on each sample to the maximum attainable temperature of its oven. In both the natural and W^{182} measurements, the heating element of the oven burned out with the sample temperature around 1420°K; the W^{186} measurement was terminated with the sample at a temperature of 1440°K because of failure of the thermocouple attached to the oven exterior. The W^{184} sample arrived late in the program; its maximum temperature was limited to 1000°K by excessive outgassing during both runs. Its oven failed during bakeout for the third run, and was not rebuilt because the high-temperature phase of the program took priority.

An example of results of a single run, together with a least-squares fit of the form $\rho = a + b\sqrt{T}$, was shown in Figure 6. The goodness of fit indicated in this figure is typical, and calculated errors of 2 to 3% in the coefficient b are not uncommon. However, the run-to-run variation is larger. This variation is tentatively attributed to variation in the goodness of vacuum, so that the empty-oven contribution may be different from run to run. In fact, the average of all measured empty-oven temperature coefficients is essentially zero, but the run-to-run variation is larger than for sample measurements. It is a matter of experience that much more difficulty is encountered in getting and maintaining a good vacuum during bakeout of empty ovens during bakeout of ovens containing samples; this is probably because of the gettering action of tungsten at high temperatures.

Inasmuch as the empty-oven temperature coefficient of reactivity was established to be zero, it was not subtracted from sample temperature coefficient, since that procedure would increase the apparent error in sample coefficients unrealistically. The error in sample coefficients calculated from deviations of individual runs from the mean should adequately describe the variation due to varying oven contributions.

Results of the Doppler-coefficient runs below 1400°K are summarized in Table 8 and are plotted in Figures 8 through 11. Also shown on the figures are calculated values of the Doppler increase in effective resonance integral, for each sample and its individual isotopes. These calculations were done by methods discussed in the next section.

TABLE 8
DOPPLER COEFFICIENTS OF TUNGSTEN SAMPLES
MEASURED BELOW 1400°K

Principal Isotope in Sample	$\sqrt{S/M}$* ($cm/gm^{1/2}$)	Maximum Temperature (°K)	$d\rho/d\sqrt{T}$ ($¢/mole-°K^{1/2}$)	Spectral Correction Factor	$dI/d\sqrt{T}$ ($barns/°K^{1/2}$)
Natural	0.457	1370	0.0051 ± 0.0002	0.899 ± 0.050	0.066 ± 0.005
182 (93%)	0.452	1370	0.00344 ± 0.00014	0.905 ± 0.048	0.0443 ± 0.0031
184 (94%)	0.460	1000	0.00319 ± 0.00010	0.90 ± 0.05	0.0408 ± 0.0026
186 (97%)	0.446	1370	0.00239 ± 0.00008	0.90 ± 0.05	0.0306 ± 0.0022

* See Table 1 for other sample properties

2. Error Discussion

The errors indicated in Table 8 for $d\rho/d\sqrt{T}$ were derived from reproducibility of repeated runs, and ranged between 3 and 4%. The 5% error assigned to the spectral correction brings the final error in $dI/d\sqrt{T}$ up to 6 to 7%.

The spectral correction factor is significantly smaller than unity because the Doppler effect takes place largely in the higher resonances, well removed from the influence of the cadmium sleeve on flux and importance, whereas the reactivity of the gold standard sample is depressed somewhat by the cadmium.

B. MEASUREMENTS EXTENDING ABOVE 1400°K

Results of reactivity measurements using the large ovens are shown in Figure 12. The principal difference from the small-oven results is readily apparent; it is the large and rapidly increasing reactivity coefficient of the empty oven. The similarity in shape to the power-vs-temperature curve suggests that the sharp increase at high temperatures may be related to increased heat losses,

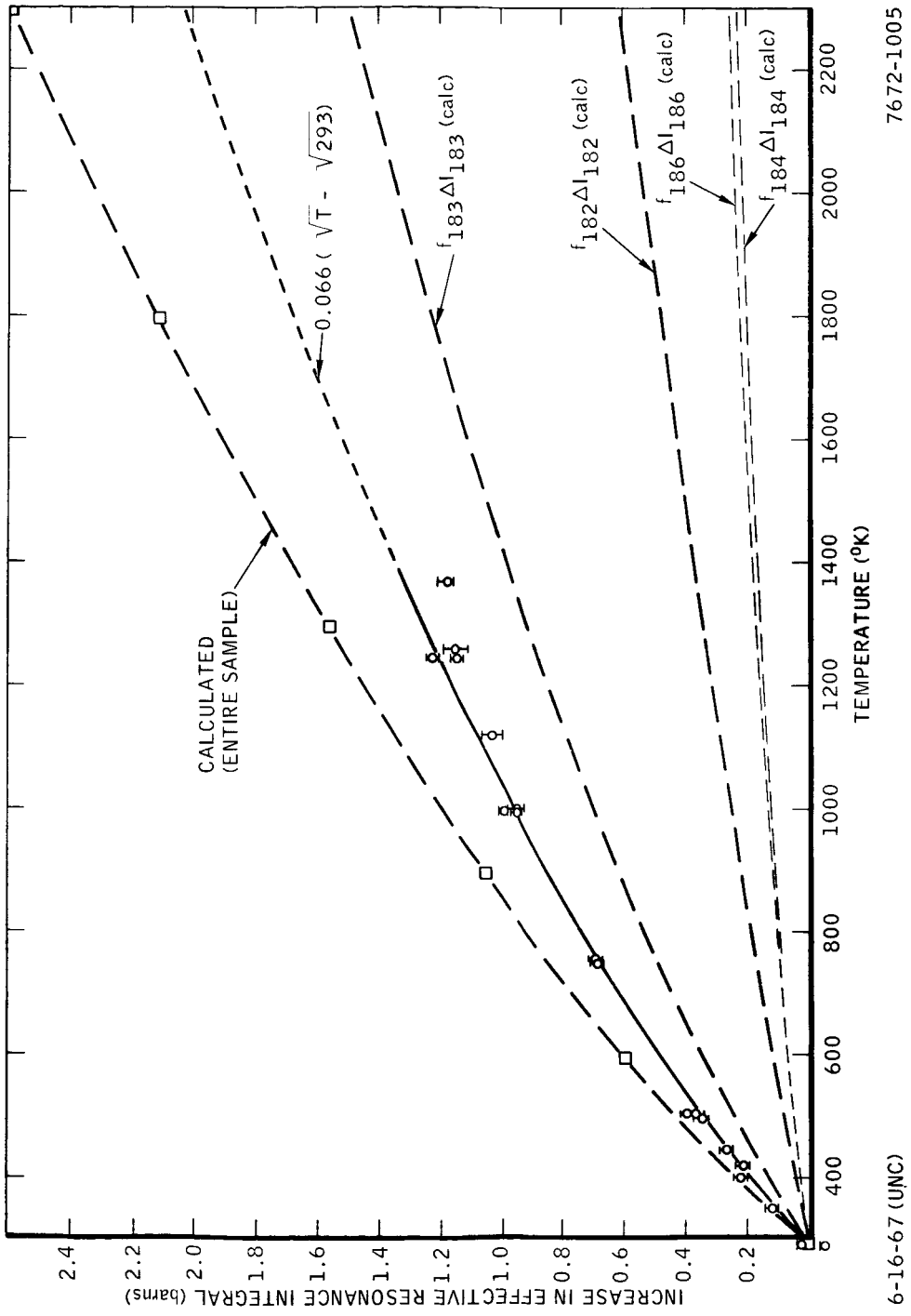

Figure 8. Comparison of Measured and Calculated Increase in Resonance Integral of Natural-Tungsten Samples vs Absolute Temperature. f_i = Atom Fraction in Sample

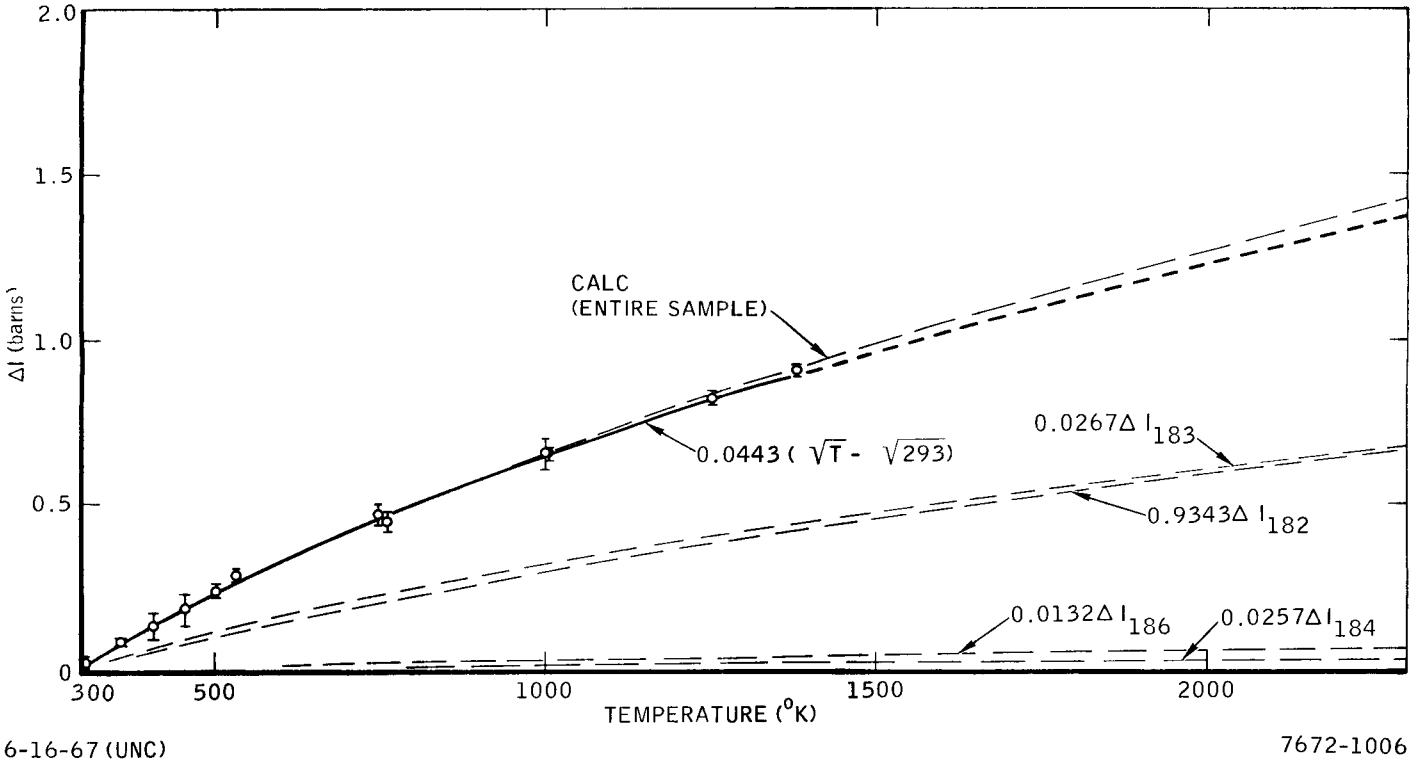

Figure 9. Measured and Calculated Increase in Resonance Integral of Tungsten Sample Enriched in W^{182}

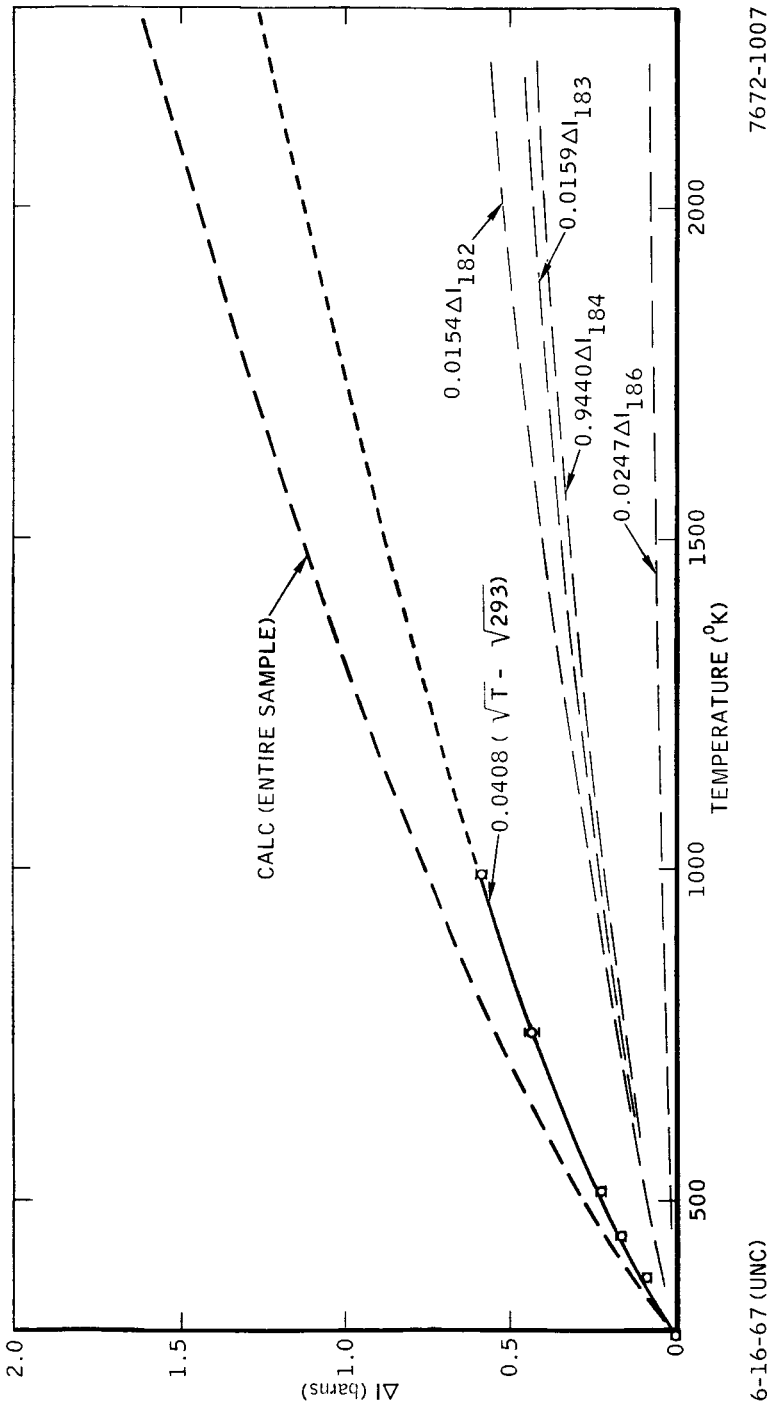

Figure 10. Measured and Calculated Increase in Resonance Integral of Tungsten Sample Enriched in W^{184}

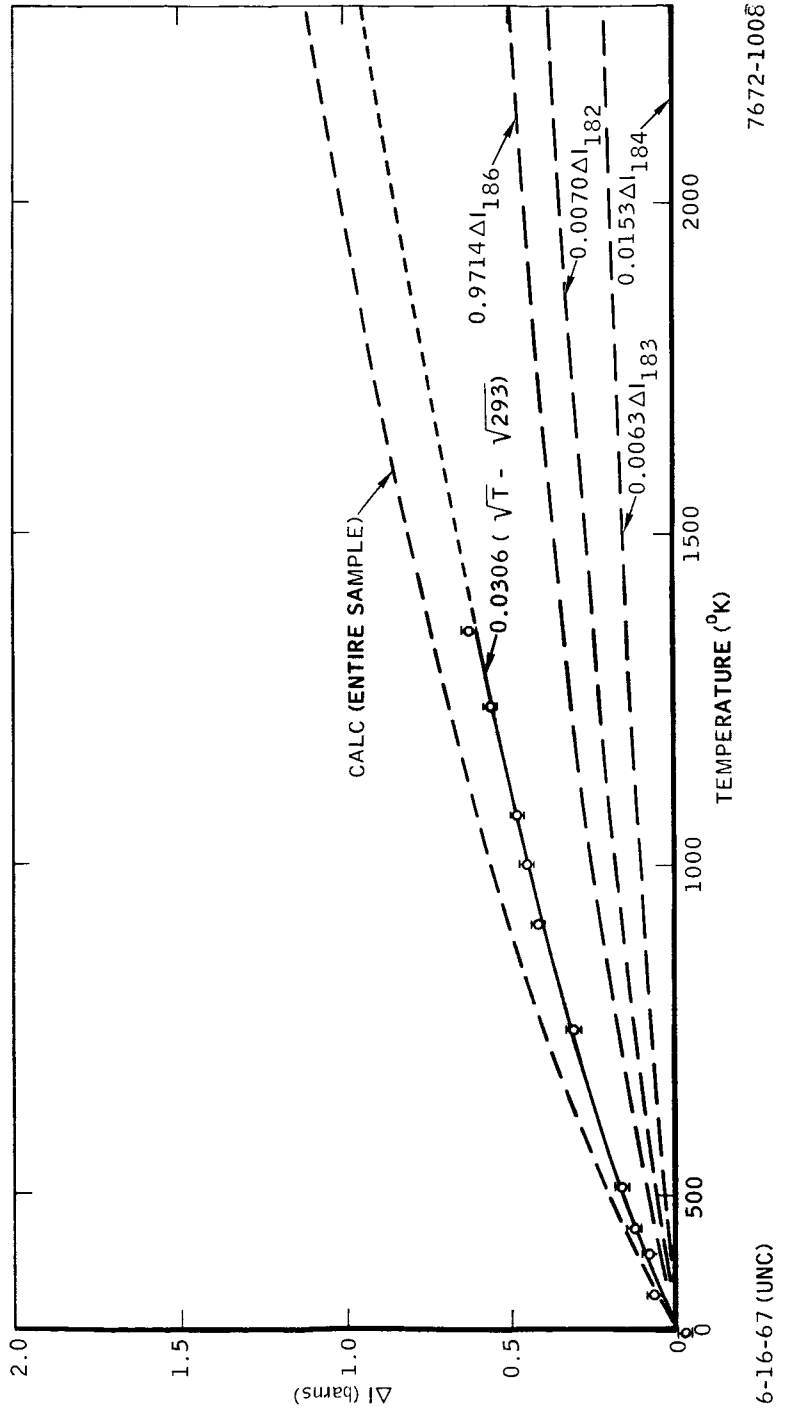

Figure 11. Measured and Calculated Increase in Resonance Integral of Tungsten Sample Enriched in W186

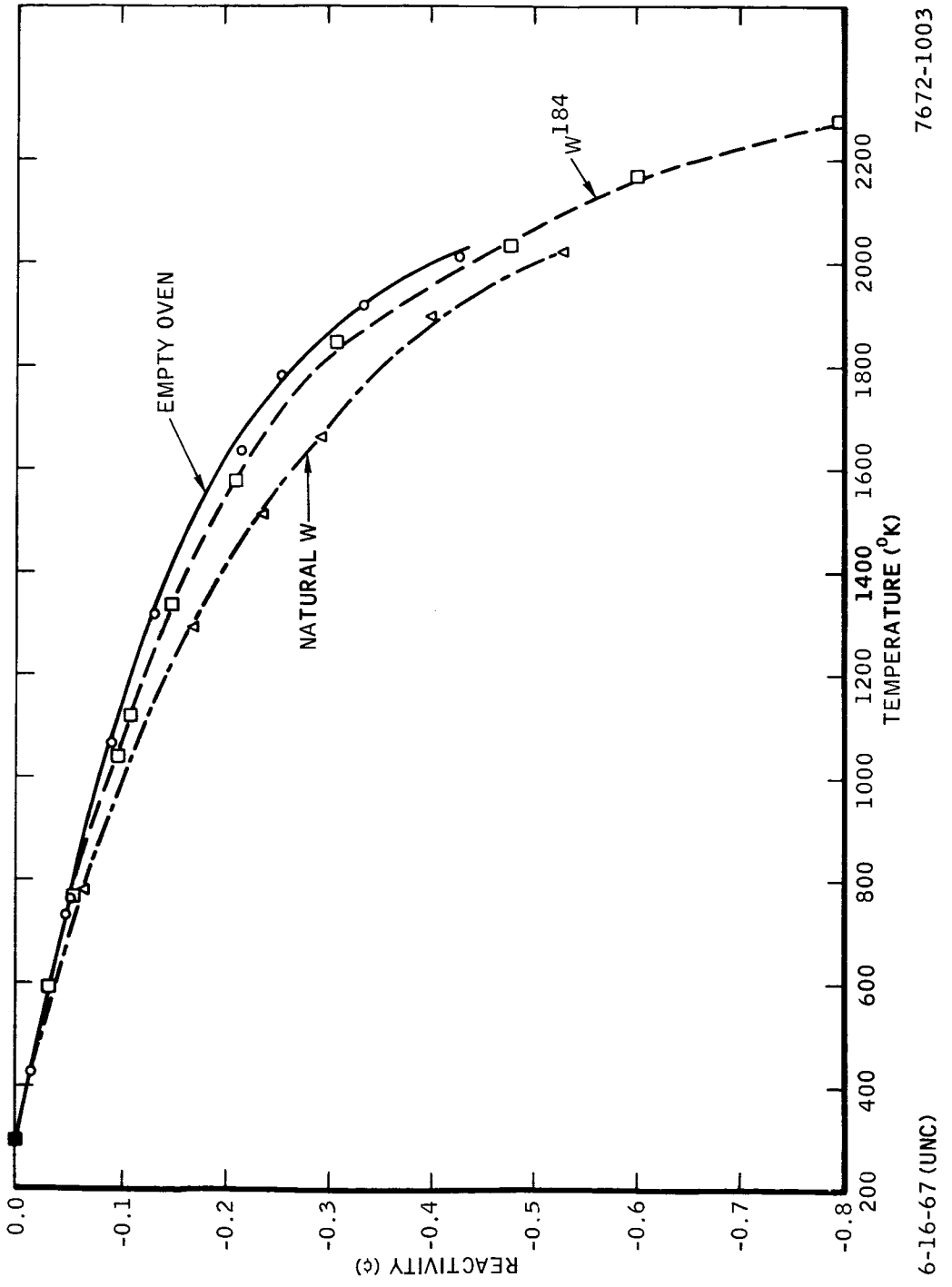

Figure 12. Results of Reactivity Measurements up to 2273 °K
(Lines shown are visual aids only and do not result from curve fits)

with attendant high temperatures of oven components. For the present, the empty-oven reactivity has simply been subtracted from the natural-tungsten and tungsten-184 reactivities. To carry out this procedure in an objective way, least-squares fits of several mathematical function were made to the empty-oven data, with temperature as independent variable and reactivity as dependent variable. The forms of the expressions used had no particular physical significance, but were chosen to be monotonic and smoothly varying.

At a given temperature, the error in the empty-oven correction was estimated from the spread in reactivities given by the different forms, since this spread was larger than the error calculated from errors in the coefficients of any one expression. For interpolation between two points where empty-oven measurements were made, the expressions agreed fairly well. As would be expected from the appearance of the empty-oven curve, however, extrapolation to 2273°K was impractical, the different expressions giving widely varying results.

Results for natural tungsten and W^{184} after making the empty-oven corrections are shown in Figure 13, along with the least-squares curves from the small-oven results. These results are clearly not of the quality of those obtained with the small ovens, due mainly to the magnitude of the empty-oven correction; both the uncorrected sample-oven reactivity change and the empty-oven reactivity change are much larger than the difference between them.

Because of the presence of considerably more absorber in the core (larger Cd sleeve plus reactivity shims in oscillator tube), the reactivity signal per sample atom was substantially reduced. The measured reactivity of the 188-gm natural-tungsten sample at room temperature was 1.21¢, compared with 1.92¢ in the previous core. Since the cadmium sleeves had the same thickness in both cores, spectral factors were unchanged, and the calibration constant for this core was given by (1.92/1.21) 14.22, or C = 22.6 mole-barns/¢.

For both the natural and W^{184} samples, the measured points below 1400°K appear unreasonably low. It seems likely that the empty-oven subtraction was too large at the lower temperatures. It was observed that oven-component temperatures were higher for a given empty-oven indicated temperature (as

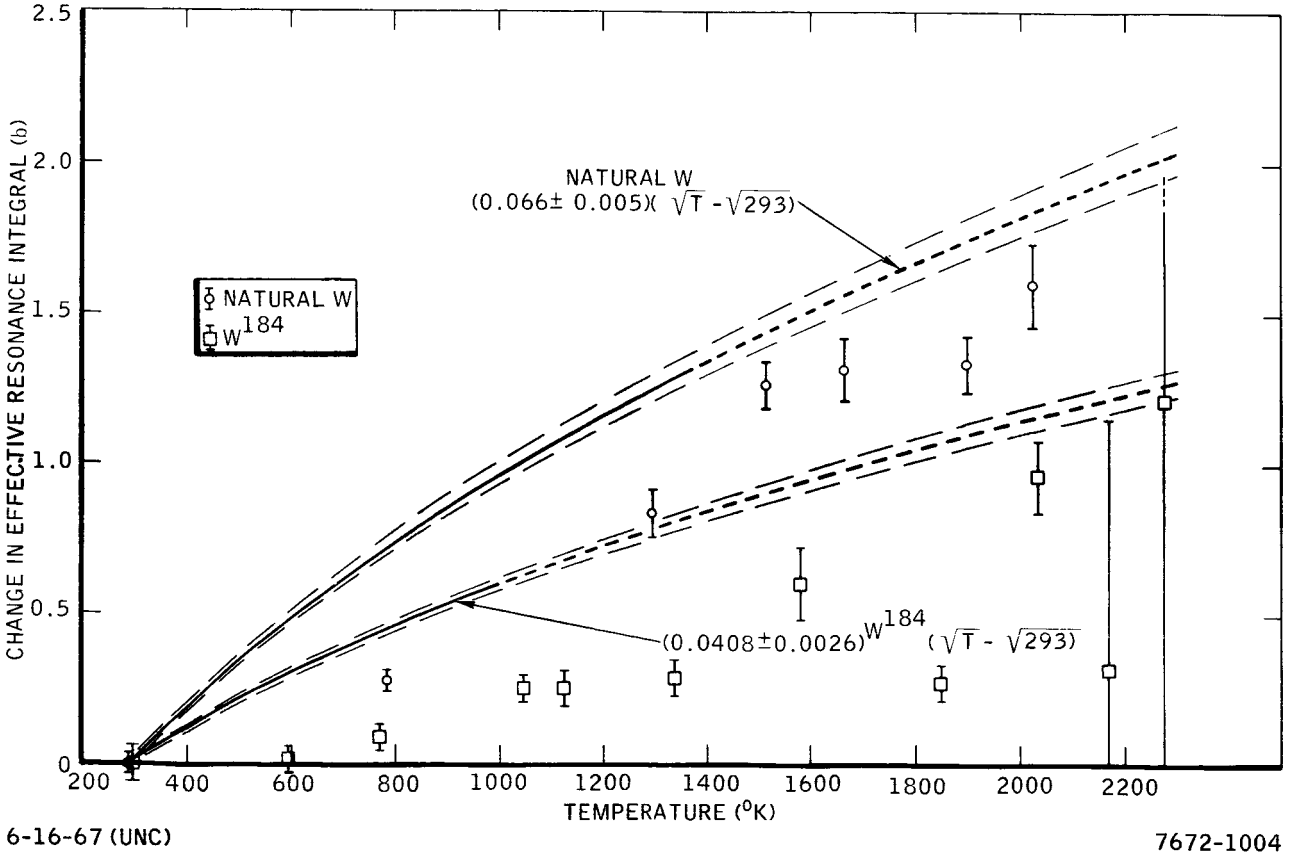

Figure 13. Results of Measurements up to 2273 °K After Empty-Oven Subtraction. (Least-squares fits to small-oven results for same samples are also shown, as solid lines up to highest measured temperature and as dotted lines above.)

measured by a thermocouple in the sample position) than for the same temperature with a sample present. These higher temperatures, caused by different heat-loss rates with and without a sample, would lead to a larger oven reactivity with a sample absent than with it present. Thus, too much reactivity would be subtracted from the total sample-plus-oven worth, and the net reactivity would be too low.

At higher temperatures, most of the power goes into heat losses, so that the presence or absence of the sample has less effect on the temperatures of the oven components. The subtraction should thus be more nearly correct. The measured points above 1400°K seem to bear out this contention.

Although it would be more desirable to find and eliminate the cause of the large oven reactivity effect, measurements with these ovens could be improved by waiting until all parts of the oven were at thermal equilibrium before measuring the reactivity.

In view of these considerations, a more reliable indication of the Doppler effect at high temperatures will be obtained from using the values of $dI/d\sqrt{T}$ measured up to 1400°K in the small ovens than from the results of measurements above 1400°K.

V. COMPARISON OF EXPERIMENTAL AND CALCULATED RESULTS

A. CALCULATIONAL METHODS

1. Analytical

Calculations of effective resonance integrals of samples as functions of temperature, geometry, and composition were carried out mainly with the TRIX-1 code.[12] With resonance parameters, atom densities, and geometry as input, this code computes Doppler-broadened effective resonance integrals and multigroup cross sections and their temperature dependence for heterogeneous or homogeneous resonance absorbers. Contributions of negative-energy, resolved, and unresolved resonances and the 1/v contribution are calculated. The single-level Breit-Wigner line shape with no overlap of neighboring resonances is assumed. The method used is essentially that of Chernick and Vernon[13] with an additional improvement in treating the resolved resonances that was developed by Goldstein and Cohen.[14] For most resolved resonances, the ratio of the practical width of the resonance to the maximum energy loss of a resonance-energy neutron in an absorber collision is neither very small (narrow-resonance approximation) nor very large (wide-resonance or infinite-mass approximation) compared to unity. The variational method of Goldstein and Cohen with linear trial functions is used to determine the location of each resolved resonance between the two extremes; the result is an analytic formula for each resonance. Unresolved resonance integrals are calculated from averages over the statistical distributions of scattering widths, using input average parameters for s-wave and p-wave resonances. An improved rational approximation to escape probabilities in lumps, applied individually to each resonance, is employed.[15] Use of a rational approximation preserves the equivalence relation between heterogeneous and homogeneous absorbers, and applying the improved approximation separately to each individual resonance increases the accuracy of both resonance integral and Doppler coefficient simultaneously. (Previous modifications of the simple Wigner approximation have applied the same correction to all resonances, improving the accuracy of either resonance integral or Doppler coefficient but not both.)

2. Monte Carlo

Monte Carlo calculations of the effective resonance integrals of a standard-sized sample of natural tungsten (0.438 in. diam, 4.0 in. long) and a gold sample (0.235 in. diam, 3.7 in. long) were performed as a check on the analytical calculations. This method did not require approximations normally used in analytic methods, such as the use of a spatially flat source in calculating sample escape probabilities, neglect of resonance overlap, flux recovery between resonances, and the narrow-resonance approximation for moderator collisions.

Routines from an existing Monte Carlo reactor code[16] were used, modified so that only neutrons crossing the sample boundary were followed. This modification resulted in greatly increased efficiency. Pointwise cross sections at 0°K were prepared from resonance parameters with the aid of the UNICORN code;[17] from these, Doppler-broadened room-temperature cross sections were calculated with the DOPCRS code.[18]

B. RESONANCE PARAMETERS

Libraries of resonance parameters for the tungsten isotopes were constructed for use in TRIX-1 and the Monte Carlo calculation. For W^{182}, W^{184}, and W^{186} these libraries were based primarily on preliminary resonance parameters derived from experiments on separated tungsten isotopes.[19] The W^{183} library was based on previously existing data. Later in the project, the results of low-energy capture measurements on tungsten isotopes became available.[20] Adjustments were made to several of the low-energy parameters so that the TRIX-1 calculation would generate the measured low-energy capture cross sections.

The adjusted resonance parameters and other necessary nuclear data for use in TRIX-1 are presented in Table 9.

TABLE 9

RESONANCE PARAMETERS FOR TUNGSTEN ISOTOPES

Isotope[+]	Resonance Number	Energy (ev)	Γ_n (ev)	Γ_γ (ev)	g
W^{182}	0	-26	*	0.055	1
$\bar{\Gamma}_{no} = 0.0171\ ev^{1/2}$	1	4.17	0.00148	0.055	1
$\bar{\Gamma}_\gamma = 0.055$ ev	2	21.1	0.0401	0.055	1
$\bar{D} = 60$ ev	3	114.7	0.290	0.055	1
Spin = 0	4	214	0.003	0.055	1
$\sigma_{pot} = 5.0$ b	5	250	1.1	0.055	1
	6	282	0.0029	0.055	1
* $\Gamma_{no} = 0.0168\ ev^{1/2}$ for negative-energy resonance	7	343	0.006	0.055	1
	8	378	0.13	0.055	1
	9	430	0.28	0.055	1
	10	486	0.5	0.055	1
	11	580	0.3	0.055	1
	12	658	0.16	0.055	1
	13	762	0.069	0.055	1
	14	922	0.4	0.055	1
	15	951	2.2	0.055	1
	16	1010	0.49	0.055	1
	17	1100	1.6	0.055	1
	18	1170	0.48	0.055	1
W^{183}	1	7.68	0.00174	0.082	3/4
$\bar{\Gamma}_{no} = 0.006\ ev^{1/2}$	2	27.1	0.0433	0.082	3/4
$\bar{\Gamma}_\gamma = 0.075$ ev	3	40.6	0.0017	0.082	3/4
$\bar{D} = 15.0$ ev	4	46.1	0.154	0.082	3/4
Spin = 1/2	5	47.8	0.115	0.082	1/4
$\sigma_{pot} = 5.0$ b	6	66.0	0.0016	0.082	3/4
	7	100.8	0.10	0.082	3/4
	8	103.8	0.012	0.082	1/4
	9	137.9	0.04	0.082	3/4
	10	144.2	0.10	0.082	1/4
	11	154.8	0.40	0.082	1/4
	12	157.1	0.067	0.082	3/4
	13	173.7	0.13	0.082	3/4
	14	192.1	0.033	0.082	3/4
	15	235.5	0.022	0.082	1/4
	16	240.4	0.014	0.082	3/4
	17	243.4	0.019	0.082	3/4
	18	259.0	0.066	0.082	3/4
	19	280.2	0.30	0.082	3/4
	20	297.6	0.044	0.082	3/4
	21	323.4	0.20	0.082	3/4

[+]The parameters $\bar{\Gamma}_{no}$, $\bar{\Gamma}_\gamma$, and $\bar{D}$, listed below each isotope, are used in calculating the contribution from unresolved resonances.

TABLE 9

RESONANCE PARAMETERS FOR TUNGSTEN ISOTOPES
(Continued)

Isotope	Resonance Number	Energy (ev)	Γ_n (ev)	Γ_γ (ev)	g
W^{183} (continued)	22	337.2	0.035	0.082	3/4
	23	348.3	0.17	0.082	3/4
	24	361.4	0.039	0.082	3/4
	25	391.6	0.043	0.082	3/4
	26	418.7	0.057	0.082	3/4
W^{184}	0	-80	*	0.055	1
$\overline{\Gamma}_{no} = 0.0285\ ev^{1/2}$	1	102.1	0.0041	0.055	1
$\overline{\Gamma}_\gamma = 0.055$ ev	2	184.7	1.2	0.055	1
$\overline{D} = 100$ ev	3	244.0	0.0023	0.055	1
Spin = 0	4	311	0.075	0.055	1
$\sigma_{pot} = 5.0$ b	5	424	0.040	0.055	1
	6	684	0.68	0.055	1
	7	787	0.06	0.055	1
	8	802	1.6	0.055	1
	9	961	1.6	0.055	1
	10	1000	0.14	0.055	1
*$\Gamma_{no} = 0.0285\ ev^{1/2}$	11	1090	3.4	0.055	1
for negative-energy	12	1140	0.34	0.055	1
resonance	13	1270	1.2	0.055	1
	14	1410	2.7	0.055	1
	15	1430	0.25	0.055	1
	16	1520	1.3	0.055	1
	17	1800	1.1	0.055	1
W^{186}	1	18.83	0.266	0.052	1
$\overline{\Gamma}_{no} = 0.01785\ ev^{1/2}$	2	171.5	0.027	0.055	1
$\overline{\Gamma}_\gamma = 0.055$ ev	3	197.6	0.0004	0.055	1
$\overline{D} = 95$ ev	4	218	0.53	0.055	1
Spin = 0	5	288	0.026	0.055	1
$\sigma_{pot} = 5.0$ b	6	407	0.075	0.055	1
	7	512	0.056	0.055	1
	8	543	0.50	0.055	1
	9	666	0.75	0.055	1
	10	732	2.2	0.055	1
	11	835	0.017	0.055	1
	12	968	1.1	0.055	1
	13	1080	0.65	0.055	1
	14	1130	0.45	0.055	1
	15	1190	0.77	0.055	1
	16	1420	0.25	0.055	1
	17	1510	1.2	0.055	1
	18	1800	0.10	0.055	1
	19	1940	0.55	0.055	1
	20	2040	0.40	0.055	1
	21	2120	0.11	0.055	1

C. COMPARISON WITH EXPERIMENT

The measurements of effective resonance integrals and Doppler coefficients discussed in Sections III and IV can serve as tests for any method of calculating these quantities. Because each tungsten isotope exhibits a different degree of dilution in each sample, a fairly wide range in dilution was covered by the samples used. The contributions from resonances of various widths and energies vary substantially with dilution, with the high-energy resonances and the $1/v$ cross sections being particularly important for thick samples (low dilution). In addition, the Doppler effect results mostly from resonances higher in energy than those that account for most of the resonance integral.

The calculational method tested here, by comparison with the experimental results, is TRIX-1. Results from this method have previously been compared with experimental results for resonance integrals and Doppler coefficients of uranium and thorium metal and oxides, with good agreement.

More recently, measurements of the resonance integral of plane samples of gold over a wide range of sample thickness have been compared with TRIX-1 calculations.[6] The calculated results are about 3% low over the entire range. Although this is reasonably good agreement, the calculated value of I for the one thick cylindrical sample measured ($\sqrt{S/M} = 0.6024$) was more than 20% high. It therefore appears that a problem exists in the application of TRIX methods to optically thick samples. For this reason, a Monte Carlo calculation of I was performed for this sample, in the manner discussed on page 47 . The result, 64.3±1.4 barns, agrees with the measured value of 63.8±1.3 barns.

1. Effective Resonance Integrals

Results of TRIX-1 calculations of the effective resonance integral of one natural-tungsten and three enriched-tungsten samples, all nominally 0.438 in. diam by 4 in. long, are presented in Table 10. Experimental results from Table 7 are repeated here for convenience. The TRIX-1 cross sections in

*Both the original Monte Carlo code and the modifications were written by L. B. Levitt. Because work on the code was terminated at an early stage, and because the version available at that stage has not been thoroughly tested, the above results must be regarded as preliminary.

the low-energy groups have been corrected for self-shielding of the 1/v cross sections with monoenergetic transport theory applied to each group, and for the change in 1/v cross section between the lower energy limit of the TRIX-1 calculation (0.414 ev) and the assumed lower energy limit of the measurements (0.622 ev).

TABLE 10

COMPARISON OF MEASURED RESONANCE INTEGRALS OF TUNGSTEN SAMPLES WITH TRIX-1 CALCULATED VALUES

Principal Isotope in Sample	$\sqrt{S/M}$* ($cm/gm^{1/2}$)	Isotopic Contribution to I† (barns/atom)				Sample I (barns)	
		182	183	184	186	Calculated§	Experimental
Natural	0.457	46.9	66.4	4.7	49.1	33.0	27.8 ±0.5
W^{182}(93.4%)	0.452	38.8	132.3	9.2	155.4	32.7	26.1 ±0.7
W^{184}(94.4%)	0.460	169.0	163.9	3.63	123.3	11.40	9.84 ±0.28
W^{186}(97.1%)	0.446	234.8	220.3	10.1	33.9	32.6	26.5 ±1.2

*Other sample properties are given in Table 1.
†For individual isotopic contributions, lower energy limit was 0.414 ev and 1/v cross section was not self-shielded.
§Total calculated sample resonance integral was adjusted to lower energy limit of 0.622 ev and 1/v cross sections were self-shielded.

In addition to the above results, the effective resonance integral of the natural-tungsten sample from 0.414 to 454 ev was also calculated with the Monte Carlo method discussed previously, with the result 27.7 ±1.0 barns. To compare with experiment, 1.4 b was subtracted for the 1/v contribution from 0.414 to 0.622 ev and 3.2 b (TRIX-1) was added for the unresolved resonances, with the result 29.5 ±1.0 barns.

The results given in Table 10 confirm the suspicion that for thick samples, some shortcomings exist in the TRIX-1 methods. There are two known effects which can be estimated, however. First, the Monte Carlo calculations of

Westfall, who compared calculations of $\underline{I}$ for natural-tungsten samples with the sum of the isotopic contributions in the sample, indicate the existence of significant resonance overlap in thick samples.[21] This was confirmed by a rough estimate of the overlap effect of the large 18.8-ev W^{186} resonance on the nearby 21.1-ev resonance in W^{182} using Kelber's method.[22] This estimate indicated that 1.8 b should be subtracted from the calculated value of $\underline{I}$ for the natural-tungsten sample for just this one resonance pair. Westfall's work indicates that calculations not allowing for overlap will be about 15% high at this S/M; this would account for most of the TRIX-1 overestimate for natural tungsten. The Monte Carlo calculation, through somewhat higher than experiment, tends to confirm this result.

The second effect, failure of the flat-source approximation for neutrons scattered in the sample, is important only for such highly scattering resonances as the 18.8-ev resonance in W^{186}. This resonance was used by Cohen in a quantitative examination of error due to the flat-source approximation.[23] For an S/M of 0.5, the effective resonance integral of the 18.8-ev resonance was overestimated by almost 20%. Corrections estimated from Cohen's results were -4.2 b for the W^{186} sample and -1.9 b for the natural sample.

Taken together, these estimated corrections remove most of the discrepancy between experiment and TRIX-1 for the natural-tungsten and W^{186} samples, but shed no light on the overestimates for the other two samples.

There appear to be two remaining possibilities. First is the possible failure of other approximations in the TRIX-1 formulation. For example, it is assumed that all resonances are narrow with respect to the maximum energy loss of a resonance-energy neutron in a moderator collision. (This should be distinguished from the usual narrow-resonance approximation, which refers to <u>absorber</u> collisions.) For carbon moderator, this assumption is violated significantly for some of the lowest tungsten resonances and the principal gold resonance as well. Failure of this approximation would lead to depression below 1/E behavior of the flux acting as source for some resonance-energy neutrons, and also to some moderator flux despression. Both effects would result in lower resonance absorption than calculated.

The second possibility involves interpretation of the experiment. If the true cadmium-cutoff energy were higher than 0.622 ev, a smaller fraction of the 1/v cross section would be measured than calculated. In thick samples such as these, the 1/v cross section can be as high as 40% of the total resonance integral. An uncertainty of 0.1 ev in cutoff energy would give rise to an uncertainty of 1 b for the W^{186} sample, 0.1 b for the W^{184} sample, and 0.5 b for the other tungsten samples. The 0.622-ev cutoff is based on an infinitely dilute 1/v absorber. The samples used deviated from both ideals, but the deviations are in opposing directions, making the true cutoff energy difficult to determine. Spectral corrections tend to reduce the effects of these deviations.

Since one or both of these effects apply to calculations for all the samples, it is possible that their inclusion might again increase the discrepancies for the natural and W^{186} samples. Thus, no one effect is likely to explain all of the differences between calculation and experiment; the TRIX-1 method simply needs further development.

2. Doppler Coefficients

Calculated increases in effective resonance integrals of both samples and individual isotopes due to Doppler broadening are given in Table 11 for a temperature increase of 1000°K. In Table 12, calculated increases in sample resonance integrals are given for temperature increases of 500, 1000, and 1500°K. From these, values of the Doppler coefficient, defined here as $dI/d\sqrt{T}$, where T is sample absolute temperature, were calculated. These values are presented in Table 13 as a function of temperature change. If the $\sqrt{T}$ temperature dependence of the Doppler effect were exact, $dI/d\sqrt{T}$ would be a constant as $\sqrt{T}$ is varied.

TABLE 11

CALCULATED INCREASES IN EFFECTIVE RESONANCE INTEGRALS DUE TO TEMPERATURE INCREASE FROM 293 TO 1293°K

Principal Isotope in Sample	Isotopic Contribution to ΔI (barns/atom)				ΔI for Sample (barns)
	182	183	184	186	
Natural	1.26	6.34	0.49	0.57	1.550
W^{182}	0.42	15.44	0.53	3.14	0.862
W^{184}	22.28	19.44	0.300	1.94	0.978
W^{186}	34.40	22.34	0.45	0.33	0.706

TABLE 12

CALCULATED INCREASES IN SAMPLE EFFECTIVE RESONANCE INTEGRALS AT VARIOUS TEMPERATURES

Principal Isotope in Sample	I(T) - I(293) (barns)		
	T = 793°K	T = 1293°K	T = 1793°K
Natural	0.906	1.550	2.087
W^{182}	0.491	0.862	1.164
W^{184}	0.578	0.987	1.310
W^{186}	0.424	0.706	0.927

TABLE 13

CALCULATED VALUES OF DOPPLER COEFFICIENT OVER VARYING TEMPERATURE RANGES

Principal Isotope in Sample	$[I(T) - I(293)] / (\sqrt{T} - \sqrt{293})$ (barns/°K$^{1/2}$)		
	T = 793°K	T = 1293°K	T = 1793°K
Natural	0.0821	0.0822	0.0826
W^{182}	0.0445	0.0457	0.0462
W^{184}	0.0523	0.0524	0.0523
W^{186}	0.0384	0.0375	0.0386

Calculated values of the Doppler coefficient are compared with measured values (from Table 8) in Table 14. The calculated values are adjusted to the same temperature range as the experiment, where necessary, by interpolation between values given in Table 13.

TABLE 14

COMPARISON OF MEASURED AND CALCULATED VALUES OF DOPPLER COEFFICIENT FOR TEMPERATURES UP TO 1400°K

Principal Isotope in Sample	$\sqrt{S/M}$	$dI/d\sqrt{T}$ (barns/°K$^{1/2}$)		Upper Temperature Limit (°K)
		Calculated	Measured	
Natural	0.457	0.0823	0.066 ±0.005	1370
W^{182}	0.452	0.0458	0.0443 ±0.0031	1370
W^{184}	0.460	0.0523	0.0408 ±0.0026	1000
W^{186}	0.446	0.0374	0.0306 ±0.0022	1370

The Doppler coefficients of all samples except W^{182} are thus significantly overestimated by the calculations. The reasons for this result are not known. The Doppler coefficient would not be affected by failure of those particular assumptions suggested previously as possible causes for calculated overestimates of effective resonance integrals, because the broad, low-lying resonances involved do not contribute significantly to the Doppler effect. Likewise, uncertainty in the cadmium-cutoff energy would not affect the Doppler coefficient, since there is essentially no change with temperature of the cross-section shape near cutoff. Most contributing resonances appear to be too well separated for resonance overlap to be significant, but this point has not been investigated quantitatively.

Probably the principal source of uncertainty in calculations of the Doppler effect is uncertainties in resonance parameters for the contributing resonances. Because these resonances are smaller than the low-lying ones, their parameters cannot be determined as accurately; indeed, a substantial fraction of the Doppler effect in thick samples such as those used in these experiments comes from the unresolved resonances.

The empirical $\sqrt{T}$ dependence of resonance absorption, usually assumed for thermal reactors, was verified by measurements carried out during this program for sample temperatures up to 1400°K. The best-fitting value of γ in the relation

$$I = a + bT^{1-\gamma} \qquad \ldots (3)$$

was determined separately for each run, and seldom differed from 1/2 by more than 0.1. Measurements between 1400 and 2273°K were too inaccurate to determine γ, but did not contradict the conclusion that $\gamma = 1/2$. As can be seen from Table 13, calculated values of the sample Doppler coefficients agreed well with the $\sqrt{T}$ law.

VI CONCLUSIONS

As outlined in the Introduction (Section I), the objective of this investigation was to measure Doppler coefficients and effective resonance integrals of natural and enriched tungsten samples to as high a temperature as possible, in a 1/E spectrum. With the obtaining of accurate measurements of Doppler coefficients of natural-tungsten, W^{182}, and W^{186} samples up to 1370°K and of the W^{184} sample up to 1000°K, this objective has been achieved.

Because of the large Doppler effect in W^{183} and the strong self-shielding of the major isotope, more than half of the calculated Doppler effect in each of the three enriched-tungsten samples was contributed by the "impurity" tungsten isotopes, having atom fractions totaling less than 7% in each sample. This result emphasizes the necessity of not neglecting any isotopes of low concentration when calculating the Doppler coefficient of reactor fuel. It also suggests that possible artificial enhancement of the fuel temperature coefficient of reactivity by introducing materials with large Doppler coefficients into the fuel, as suggested in some reactor designs, may require much smaller amounts of material than would normally be estimated.

With regard to experimental techniques, it was determined that the dynamic or power-history method of measuring reactivity, previously used only for routine measurements such as rod calibration, was capable of refinement to the point where the precision of small-sample reactivity measurements approached the theoretical limit set by reactor noise. It was also demonstrated that the small, sealed-off ovens developed for heating samples in a fast critical assembly could be used in a 1/E spectrum in a thermal critical assembly while introducing very little reactivity variation with temperature, principally because of the small amounts of extraneous material and the low power requirements (100 watts for 1370°K) of these ovens.

The calculational procedure used during this program was found to overestimate both resonance integrals and Doppler coefficients by as much as 25% for some samples. Overestimation of the Doppler effect may be due

to uncertainties in resonance parameters, particularly in the unresolved region, as the calculated Doppler coefficient is very sensitive to these parameters. Resonance overlap in natural tungsten and failure of the flat-source approximation in W^{186} can account for most of the discrepancy in calculated resonance integrals for these two samples. Possible sources for the discrepancies in other samples include uncertainty in the cadmium-cutoff energy and failure, in broad resonances, of the narrow-resonance approximation for moderator scattering. It is unlikely that any one effect is solely responsible for these discrepancies. Indeed, it is possible that consistent application of additional corrections to calculations for all samples might invalidate the near-agreement achieved for natural tungsten and W^{186} by correcting only for resonance overlap and spatial source variation. It thus appears that the TRIX-1 methods, originally intended for survey calculations because of speed and convenience, need further development if detailed agreement with experiment is expected.

Probably the most significant conclusion to be drawn from these measurements concerns the temperature dependence of the Doppler coefficient in a 1/E spectrum. The accuracy of measurements made with the small ovens was sufficient, over the temperature range 300 to 1370°K (1000°K for W^{184}), to allow making a clearcut choice between the form

$$I = a + b\sqrt{T}, \qquad \ldots (4)$$

suggested by the results of many calculations, and the older form

$$I = a + bT, \qquad \ldots (5)$$

which could not be ruled out entirely by previous measurements. The results of this experiment clearly favor the square-root form of the Doppler temperature dependence.

VII. APPENDICES

A. CALCULATED CORRECTIONS TO EXPERIMENTAL RESULTS

1. Spectrum Calculations

Spectra of the real and adjoint neutron fluxes at the sample position were obtained from a 15-group, one-dimensional analysis of the SGR-CA 10.6-in. lattice. Thermal-group constants were obtained from a previous THERMOS analysis by Fillmore.[24] The library value of the thermal absorption cross section for graphite was adjusted to the value measured by DeJuren and Stewart[25] for the particular AGOT graphite in the SGR-CA. In each fast group, the value of ν for U^{238} was adjusted to mock up the transport-theory correction to fast fission in a lattice.[26] Group cross sections for U^{235} and U^{238} in the resonance region were calculated with TRIX.

The 15-group analysis was done with CAESAR,[27] a multigroup diffusion-theory code. Quantities calculated included neutron lifetime (1.240 msec), β_{eff} (0.007035), and critical size. The critical loading resulting from this calculation was 20.0 fuel elements, which agreed well with the actual loading of 19.4 elements. (Although the standard loading in this lattice was 21 elements, each of the three outer elements was only partially loaded with fuel.)

These calculations were performed with a 1.33-in.-diam central axial void in the SGR-CA, both with and without a cadmium sleeve, 1.33 in. OD and 1.27 in. ID. Because the calculation was one-dimensional, the sleeve was implicitly assumed to have the full core height, 96 in. Although the actual sleeve height was only 6 in., it follows from both solid-angle arguments and the results of experiments with and without cadmium end caps that this approximation should not lead to appreciable error. (The possible extent of error is discussed in Section III-D.)

The resulting spectra of the real flux and adjoint flux (importance) at the sample position are presented in Table 15.

TABLE 15

CALCULATED SGR-CA NEUTRON SPECTRA AT SAMPLE POSITION

Group No.	Upper Energy Limit	No Cadmium Sleeve		Cadmium Sleeve	
		Real Flux*†	Adjoint Flux*	Real Flux*†	Adjoint Flux*
1	10.0 Mev	0.0732	0.8453	0.0723	1.0850
2	3.0 Mev	0.6784	0.8335	0.6675	1.0528
3	1.4 Mev	0.8031	0.8494	0.7914	1.0453
4	0.9 Mev	1.1908	0.8672	1.1811	1.0513
5	0.4 Mev	0.7930	0.8942	0.7890	1.0568
6	0.1 Mev	0.8580	0.9138	0.8521	1.0538
7	17. kev	0.9241	0.9348	0.9140	1.0463
8	3.354 kev	0.9742	0.9539	0.9618	1.0377
9	454. ev	0.9964	0.9775	0.9866	1.0242
10	61.44 ev	1.0000	1.0000	1.0000	1.0000
11	22.6 ev	0.9977	1.0087	1.0094	0.9671
12	8.3 ev	0.9888	1.0146	1.0047	0.9005
13	3.06 ev	0.9767	1.0168	0.9702	0.7700
14	1.126 ev	0.9631	1.0152	0.4696	0.3568
15	0.414 ev	-	-	-	-

* Relative to Group 10
† Per unit lethargy

The cadmium sleeve was put into the calculational model explicitly. Ten mesh points were used across its 0.031-in. thickness. The thermal (group 15) cross section was calculated by averaging pointwise data over a carbon spectrum calculated with TEMPEST.[28] Cross sections for both groups 15 and 14 were multiplied by a factor of 0.86 to correct for the difference in flux depression between diffusion theory and transport theory. This factor was computed from a model consisting of an infinite slab of cadmium in an infinite graphite medium. The final values of σ_a (Cd) put into CAESAR were 2600, 118, and 4.0 b, for groups 15, 14, and 13, respectively. Cross sections for the low epithermal groups (12-14) were obtained by averaging pointwise data

from the Aldermaston nuclear-data tape over a 1/E spectrum. Cross sections for higher-energy groups were averaged over a carbon spectrum calculated with FORM.[29] The cadmium resonance integral was assumed to be 40% of its infinitely dilute value; results are insensitive to this assumption.

The most significant effect of the cadmium on the spectra is seen in Table 15 to be the reduction of the importance function for the low-energy epithermal groups. This reduction is readily understood on physical grounds: an epithermal neutron in the sleeve has a good chance of returning to the sleeve and being captured as a thermal neutron after several collisions in the graphite, rather than causing a fission in one of the nearest fuel elements, nine inches away. (Recall that the importance of a neutron with a given energy and position is proportional to the probability that that neutron will eventually cause a fission.)

2. Spectral Corrections

The effective resonance integral, I, is defined as the cross section that yields the correct absorption rate in the resonance region when multiplied by the unperturbed flux per unit lethargy in the resonance region, assumed to be constant (i.e., proportional to 1/E on the energy scale). Thus,

$$\phi_0 I = \int_0^{u_c} \phi_0 G(\sigma)\, \sigma(u)\, du, \qquad \ldots (6)$$

where ϕ_0 is the constant flux per unit lethargy in the absence of the absorber, $u = \ell n(10^7/E)$ is the lethargy, $\sigma(u)$ is the absorber cross section, and $G(\sigma)$ is a flux-reduction factor accounting for self-shielding in the absorber volume. The right-hand side of Equation (6) is the total absorption rate in the lethargy region below some cutoff u_c (above the cutoff energy E_c).

The reactivity change caused when a sample of resonance absorber is placed in a cadmium shield in a reactor is given by

$$C\rho = \int_0^{u_c} \phi(u)\phi^*(u)G(\sigma)\sigma(u)du, \qquad \ldots (7)$$

where C is a proportionality constant, ϕ^* is the importance, and u_c is the cutoff lethargy defined by the cadmium shield. Clearly, if both ϕ and ϕ^* are independent of lethargy, the reactivity ρ will be directly proportional to the effective resonance integral of the sample.

Define a quantity $J = C\rho$, assuming C is known. J is nearly equal to I if the reactor has an approximately 1/E energy spectrum and lethargy-independent importance. The spectral correction factor, f, is defined as the quantity that multiplies the wrong answer (J) to give the right answer (I), thus: $I = fJ$.

At present, f can be determined only analytically, by calculating I from the resonance parameters and sample size and J from the calculated I(u) and the calculated spectrum $\phi(u)\phi^*(u)$. Let $\psi(u) = \phi(u)\phi^*(u)$ and let the self-shielding factor $G(\sigma)$ be incorporated into an effective cross section $\sigma(u)$. Then

$$f = \frac{I}{J} = \frac{\psi_o \int \sigma(u)du}{\int \psi(u)\sigma(u)du}, \qquad \ldots (8)$$

where ψ_o is the normalizing factor for ψ and the integrals have the same limits as before.

The calibration constant C is determined experimentally by measuring ρ for a sample with known I and correcting the result with a calculated value of f:

$$C = I_s/\rho_s f_s, \qquad \ldots (9)$$

where the subscript s refers to the standardizing sample. For an unknown sample x, $I_x = f_x C\rho_x$, or

$$I_x = (f_x/f_s)C(\rho_x/\rho_s), \qquad \ldots (10)$$

so that the normalization ψ_0 in $\underline{f}$ cancels out, and its choice is arbitrary. The choice made here was to normalize ψ to the total lethargy width over which $\underline{f}$ was calculated, namely groups 7 through 14 of Table 15 (17 kev to 0.414 ev).

Correction factors for this experiment were calculated with Equation (8) above, using ϕ and ϕ^* from Table 15 and multigroup cross sections calculated with TRIX-1.

It is difficult to estimate errors in these spectral correction factors. There will be partial error cancellation, since all calculated quantities ($\psi(u)$, $\sigma_s(u)$, and $\sigma_x(u)$) appear under integral signs in both numerator and denominator of the right-hand side of Equation (10). Work by Kaufman and Foell indicates that diffusion theory overestimates the importance depression caused by cadmium in the ARMF-II critical assembly.[30, 31] If this is true in general, correction factors calculated with transport theory would be closer to unity than those computed from the spectra given in Table 15, even though the latter resulted from cadmium cross sections adjusted to agree with a transport calculation.

3. Miscellaneous Effects

a. Thermal Expansion

Thermal expansion of the sample increases its total absorption by decreasing the self-shielding of both the resonance and 1/v cross sections. Estimates of the self-shielding decrease of the 1/v portion were made with the aid of Wigner's rational approximation to the escape probability of a lump.[32]

With the notation used in this report, this approximation takes the form

$$G(E) = \frac{1}{1 + \sigma(E)/s} . \qquad \ldots (11)$$

If this expression for G is substituted into Equation (6) with a 1/v energy dependence of σ, the result of the integration gives the approximate contribution of the 1/v cross section, I_v, to the total effective resonance integral. This result is

$$I_v(s, E_c) = 2s \ln(1 + \sigma_c/s), \quad \ldots (12)$$

where σ_c is the value of the 1/v cross section at the cadmium-cutoff energy E_c. Differentiation leads to the approximate result

$$\frac{1}{I_v}\frac{dI_v}{dT} = \frac{2\alpha}{1 + s/\sigma_c}, \quad \ldots (13)$$

where α is the linear thermal-expansion coefficient.

The thermal-expansion coefficients of I_v were estimated for the tungsten samples with Equation (13) and yielded results that were small compared with experimental errors in the Doppler coefficients.

Thermal-expansion effects on I were estimated from the calculated dependence of I on s and the relation

$$\frac{ds}{dT} = 2\alpha s . \quad \ldots (14)$$

These results were also small compared with experimental errors.

b. Self-Shielding of 1/v Cross Sections

In most resonance-integral codes, the 1/v contribution to the resonance integral (or to the group cross sections) is assumed to be infinitely dilute. Thus, the effective resonance integral consists of a large, geometry-dependent term and a small, additive, constant term. Although this approximation is excellent in most cases, it is obviously not very good

when the lump is so thick that the 1/v contribution is a reasonable fraction of the total calculated resonance integral. This is the case for standard-sized tungsten samples.

Equation (12) was used to estimate the self-shielding decrease of I_v in natural tungsten, which turned out to be 0.73 b. This method was not used in the TRIX-1 calculations, however. Instead, self-shielding corrections were computed with monoenergetic transport theory for each energy group in which the 1/v cross section was appreciable.

B. DESCRIPTIONS OF DATA-ANALYSIS CODES

1. RHOAV - A Code to Calculate Average Reactivity Differences from Reactor Power Changes

The code RHOAV, written in FORTRAN IV, was used to analyze nearly all data produced in this project. From the power history of the critical assembly during slow oscillation of the sample, this code calculated the reactivity at each time step, the average reactivity and standard deviation for each half-cycle of oscillation, the average and standard deviation of the reactivity difference between sample-in and sample-out positions for each complete cycle and for each equiphase point in all cycles, and finally the weighted mean, internal, and external errors for the reactivity difference over all cycles. RHOAV is the result of modifying an existing reactivity code,[9] used mainly for rod calibrations and other routine reactivity measurements of small reactivity changes. The usual source-free reactor-kinetic equations are transformed into the following integrodifferential equation:

$$\frac{\rho}{\beta} = 1 + \frac{\frac{\ell}{\beta}\frac{dn}{dt} - \sum_i a_i e^{-\lambda_i t}\left[n_o + \lambda_i \int_o^t k(t')n(t')e^{\lambda_i t'}\,dt'\right]}{k(t)\,n(t)} \qquad \ldots (15)$$

where ρ is the reactivity, β is the effective delayed-neutron fraction, k is the effective multiplication constant, n is the number of neutrons in the reactor (or a quantity proportional to it), ℓ is the neutron lifetime and a_i, λ_i are the relative abundance and decay constant of the $i^{\underline{th}}$ precursor group.

Thus, the reactivity in dollars (ρ/β) can be found from multichannel-analyzer data yielding n(t) in a quantized form. The time integral is carried out only once for each channel; this answer is then saved to be used in the next time step. The relatively wide (2-sec) channels used in this experiment require a nonconstant n(t) in the integral across a channel; in RHOAV, n(t) in the $m^{\underline{th}}$ channel is approximated by an exponential whose slope is determined from the number of counts in the $(m+1)^{\underline{th}}$ and $(m-1)^{\underline{th}}$ channels and whose amplitude is such that the integral over n(t) in the $m^{\underline{th}}$ channel equals the number of counts in that channel.

In a typical oscillator run with a 400-channel analyzer, some 225 channels yield useful information, the remainder corresponding to times when the oscillator was moving. The reactivities calculated for each of these 225 channels are used to compute the average in-out reactivity difference and its standard deviation. They are also combined in various ways to yield statistical information about consistency of individual cycles with the mean and about possible time-dependent or phase-dependent trends.

Figures 14 through 17 are examples of graphical output from RHOAV.

Running time on the IBM 7094 is approximately 7 sec per 400-channel case.

2. DOPFIT* - A Code to Determine the Best-Fitting Temperature Dependence for the Doppler Effect

Once the reactivity of a sample was determined at a number of temperatures, the DOPFIT code was used to determine the exponent γ in the following expression assumed to represent the temperature dependence of the Doppler effect:

$$\rho = a + bT^{1-\gamma} , \qquad \ldots (16)$$

*Written by R. J. Tuttle of Atomics International. No documentation is available.

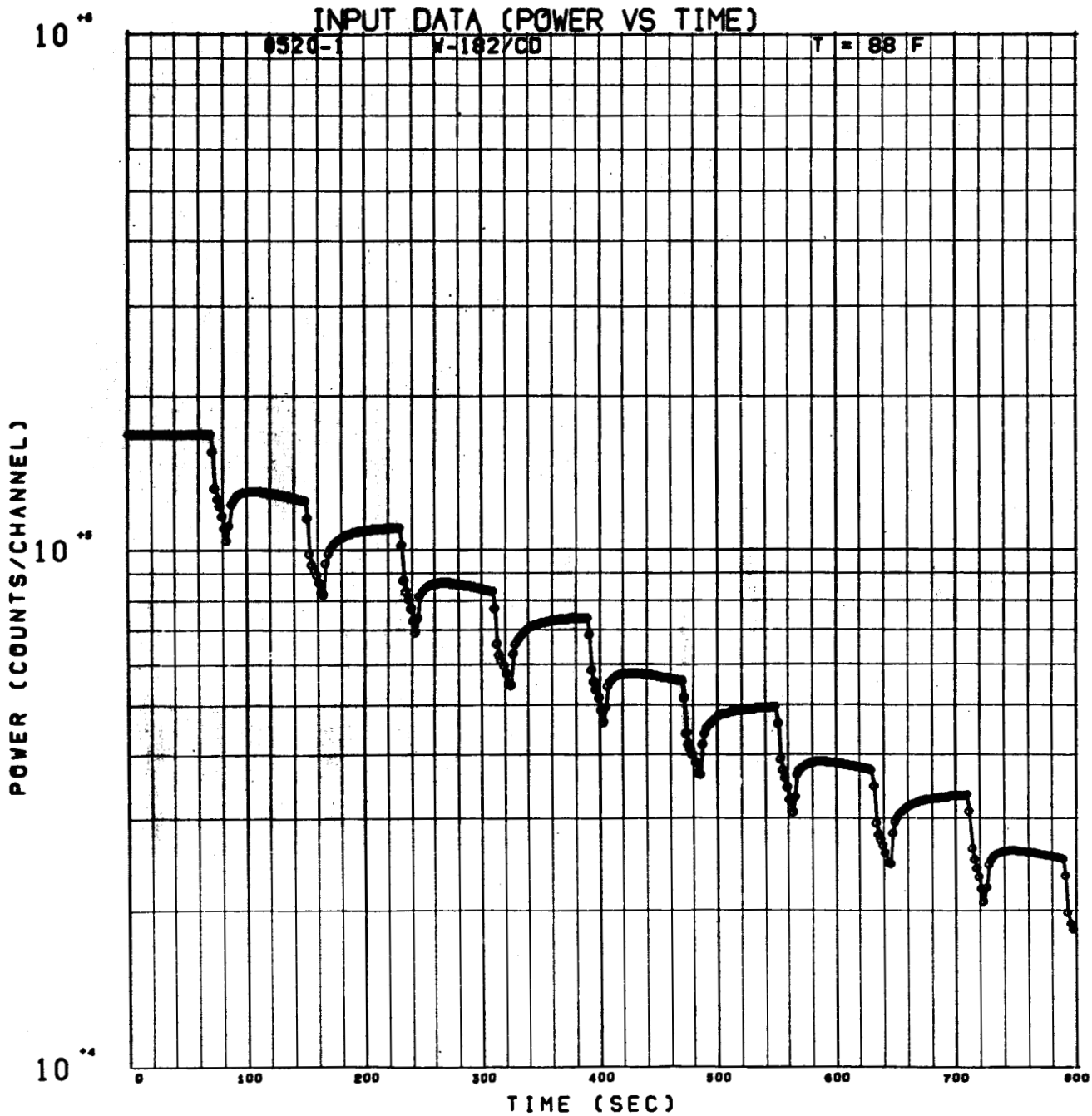

Figure 14. Power History from Typical Oscillator Run (0520-1)

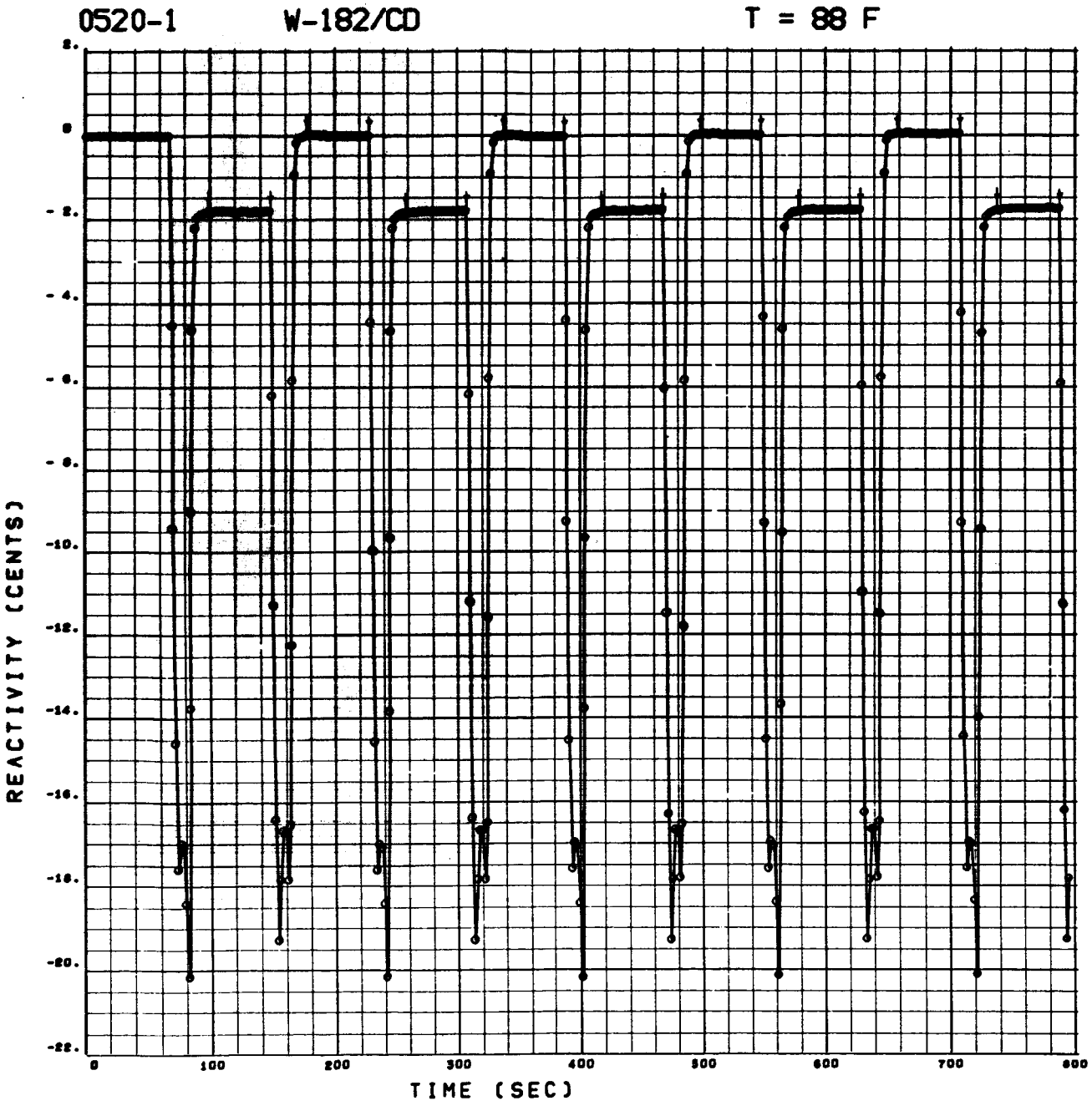

Figure 15. Reactivity vs Time Determined from Power History for Run 0520-1 (Room Temperature)

Points used in determining average reactivities over level portions of cycle are those between arrows shown on graph.

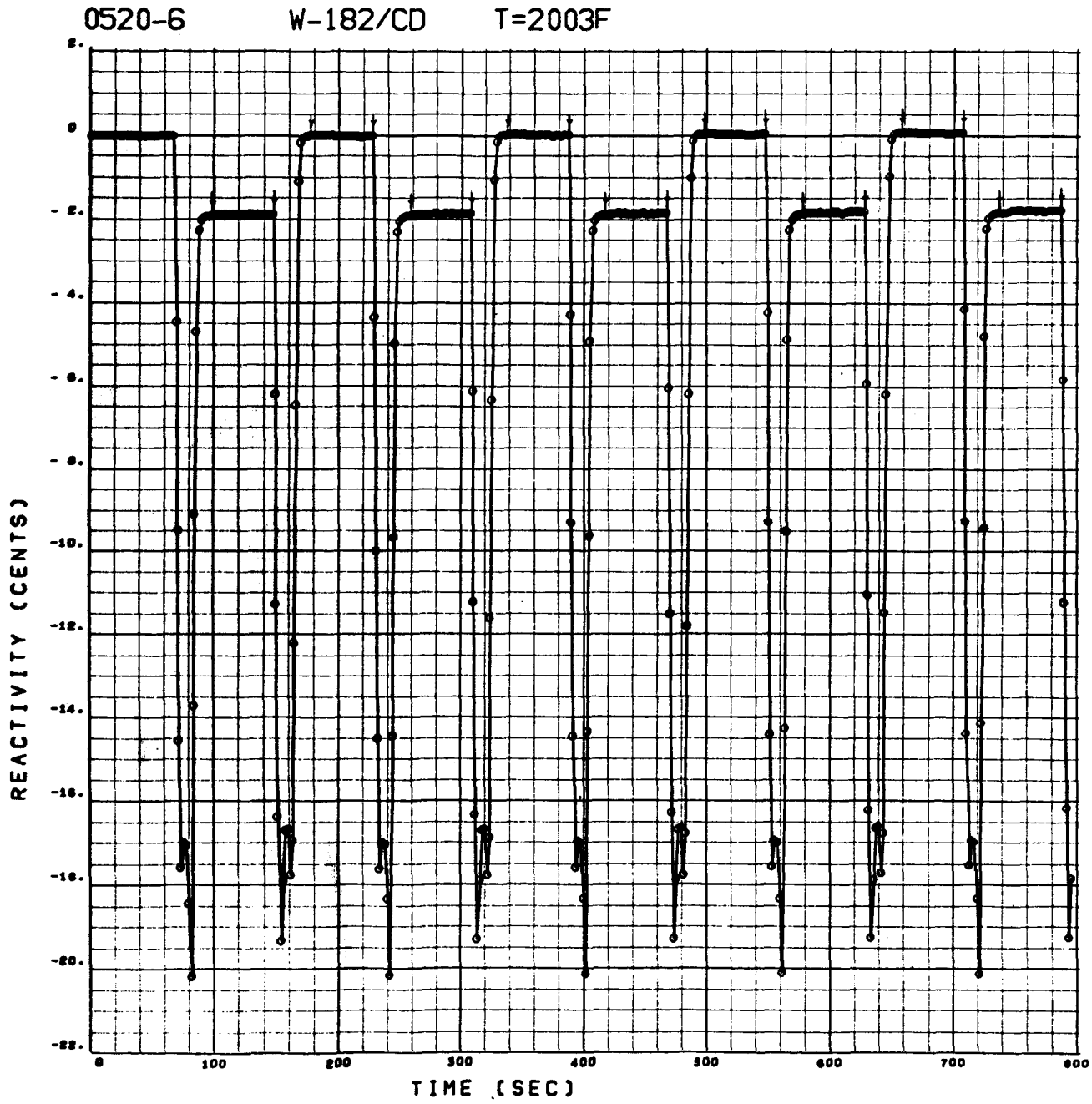

Figure 16. Reactivity vs Time Determined from Power History for Run 0520-6 (1368°K)

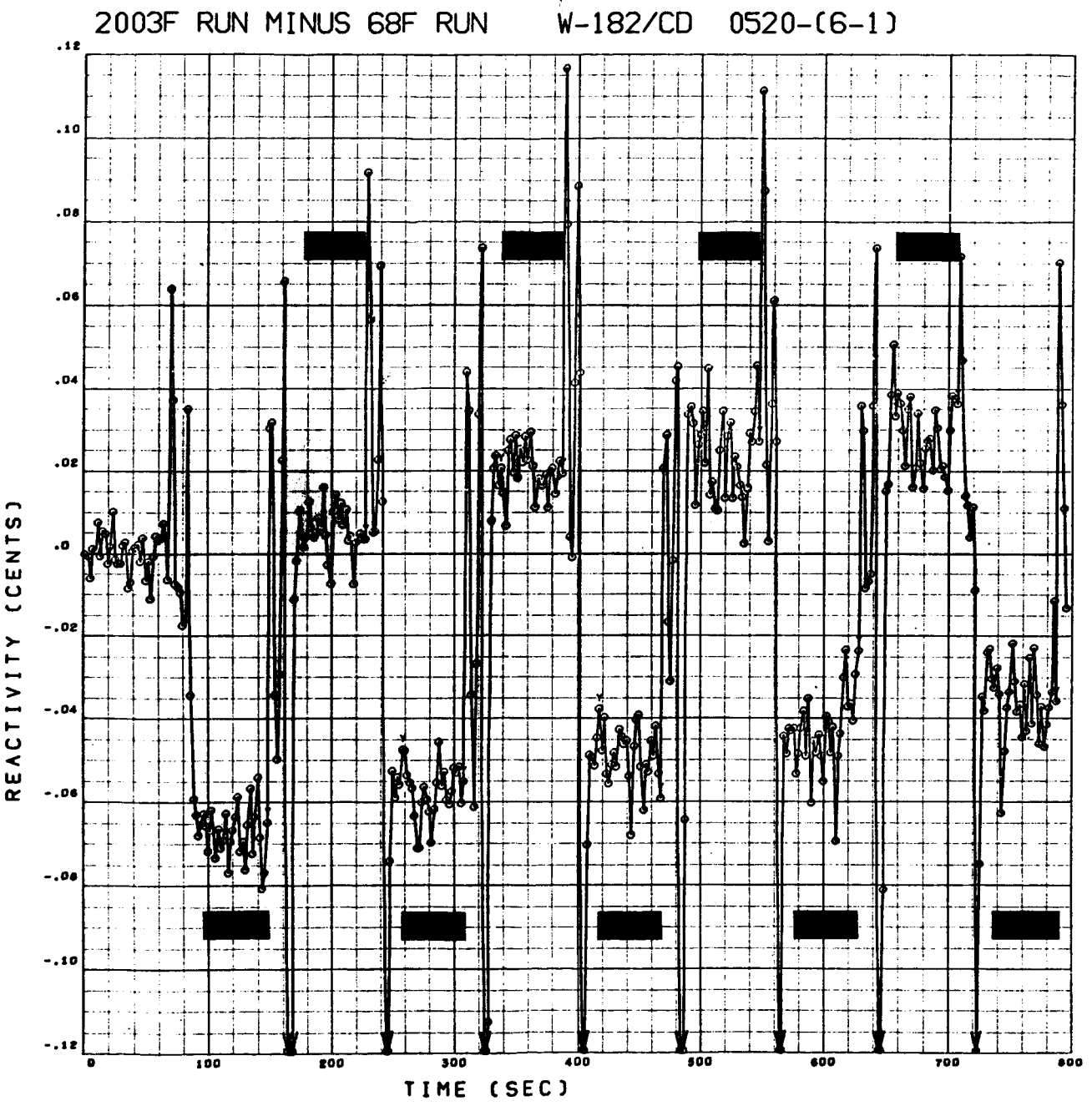

Figure 17. Pointwise Reactivity Difference, 1368°K Run Minus Room-Temperature Run, Magnified Scale

Solid bars indicate time spans over which average reactivity differences were determined. Note size of statistical fluctuations over level portions of cycle. Precision of reactivity difference for this measurement was better than 0.002¢.

where ρ is reactivity, T is temperature in degrees Kelvin, a and b are least-squares constants determined from the experimental points and errors, and γ is allowed to vary from 0 to 1.5 in a search for the minimum weighted least square of the sum of the deviations of the calculated values from the experimental ones. For a thermal reactor, γ is expected to be of the order of 0.5; for fast reactors, it is usually taken to be 1 (in which case $\rho = a + b \ln T$) or 1.5. DOPFIT was written (in FORTRAN IV) for the AEC-sponsored Fast Doppler Measurements program at Atomics International.

Input to DOPFIT consists of title, void-correction and expansion-correction options (none, linear, or pointwise) and γ-search option on the first card; normalization data, input-temperature scale options (C, K, or F) and scale limits on the second card; then all temperatures, all reactivities, and all reactivity errors for the experimental points; then the data for void (empty oven) and expansion corrections, if any. Printed output consists of the best least-squares-fit values of $\underline{a}$ and $\underline{b}$ and the expected and observed values for the rms error of the fit, for each value of γ ranging from 0 to 1.5 in 0.1 steps (or in 0.01 steps about a specified value of γ, if that option was chosen). Graphical output consists of a plot of the best-fitting curve together with the experimental points and errors, and a plot of the rms error of fit as a function of γ. Running time on the IBM 7094 is about 7 sec per case.

Figure 6 is an example of the graphical output of DOPFIT.

REFERENCES

1. R. M. Pearce, "The Doppler Effect in Thermal Reactors," J. Nucl. Energy, Part A, 13, 150-175 (1961).

2. L. W. Nordheim, "The Doppler Coefficient," Chapter 4 in Vol 1 of The Technology of Nuclear Reactor Safety, T. J. Thompson and J. G. Beckerley, eds. The MIT Press, Cambridge, Massachusetts (1964).

3. A. R. Vernon, "Calculation of the effective resonance integral of U238," Nucl. Sci. Eng. 7, 252-259 (1960).

4. E. Hellstrand, P. Blomberg, and A. S. Horner, "The temperature coefficient of the resonance integral for uranium metal and oxide," Nucl. Sci. Eng. 8, 497-506 (1960).

5. D. Bogart and E. Lantz, "Nuclear Physics of Solid-Core Gas-Cooled Rocket Propulsion Reactors," NASA-SP-11, Vol. 2 (December 1962)

6. Calculations by J. M. Otter, reported by L. S. Beller and H. Farrar IV, "A Wide Range Study of the Effective Resonance Integral and Doppler Effect in Au^{197}," NAA-SR-Memo-11511 (July 1965).

7. T. H. Springer and S. G. Carpenter, "A Measurement of the Doppler Effect in Thorium in a Fast Neutron Energy Spectrum with a Median Fission Energy of 190 kev," Nucl. Sci. Eng. 17, 194-199 (1963); T. H. Springer, S. G. Carpenter, and R. J. Tuttle, "Fast-Spectrum Doppler Measurements - Part II: A Measurement of a Negative Doppler Effect in U^{235} and New Measurements in Th^{232} and U^{238}," Nucl. Sci. Eng. 20, 272-280 (1964).

8. R. W. Campbell et al, "Critical Experiments on Slightly Enriched Uranium Metal Fuel Elements in Graphite Lattices," NAA-SR-7541 (June 30, 1963).

9. S. G. Carpenter, "Reactivity Measurements in the AETR Critical Experiments," Nucl. Sci. Eng. 21, 429-440 (1965).

10. B. J. Toppel, "Sources of Error in Reactivity Determinations by Means of Asymptotic Period Measurements," Nucl. Sci. Eng. 5, 88-98 (1959).

11. R. W. Stoughton, J. Halperin, and Marjorie P. Lietzke, "Effective Cadmium Cutoff Energies," Nucl. Sci. Eng. 6, 441-447 (1959).

12. J. M. Otter, "The TRIX-1 Code, an Improved Analytical Calculation of Resonance Integrals," NAA-SR-Memo-11538 (July 26, 1965).

13. J. Chernick and R. Vernon, "Some Refinements in the Calculation of Resonance Integrals," Nucl. Sci. Eng. 4, 649-672 (1958).

14. R. Goldstein and E. R. Cohen, "Theory of Resonance Absorption of Neutrons," Nucl. Sci. Eng. 13, 132-140 (1962).

15. J. M. Otter, "Escape Probability Approximations in Lumped Resonance Absorbers," NAA-SR-9744 (1964).

16. L. B. Levitt, "SAFE -- A Three Dimensional Monte Carlo Code to Perform Safety Analysis of Fuel Elements. Part I, Theory and Methodology," AI-65-Memo-95 (November, 1965).

17. J. M. Otter, "UNICORN -- A Program to Calculate Point Cross Sections from Resonance Parameters," NAA-SR-11980, Vol VI (June 30, 1966).

18. C. L. Dunford and E. L. Bramblett, "DOPCRS, A Code to Doppler Broaden Resonance Data for Monte Carlo Calculations," AI-CE-Memo-21 (June 20, 1966).

19. J. E. Russell, R. W. Hockenbury, and R. C. Block, "Neutron Capture Cross Section Measurements of the Tungsten Isotopes," Annual Technical Report (FY 1965), Linear Accelerator Project. Rensselaer Polytechnic Institute (1965).

20. S. J. Friesenhahn, E. Haddad, F. H. Frohner, and W. M. Lopez, "The Neutron Capture Cross Section of the Tungsten Isotopes from 0.001 to 10 Electron Volts," GA-6882 (January 20, 1966).

21. R. M. Westfall, "Resonance Overlap in Natural Tungsten," Trans. Am. Nucl. Soc. 9, 504-505 (1966).

22. C. N. Kelber, "A Simple Estimate of the Effects of Resonance Interference," Nucl. Sci. Eng. 22, 120-121 (1965).

23. S. C. Cohen, "An Improved Treatment of Scattering Resonances in Slab Geometry," Nucl. Sci. Eng. 27, 133-135 (1967).

24. F. L. Fillmore, "Thermal Neutron Spectrum Effects on Calculations for Graphite Lattices," NAA-SR-7892 (October 15, 1964).

25. J. A. DeJuren, T. E. Stewart, and E. R. Specht, "Measurements of Thermal Neutron Absorption Cross Section and Diffusion Length of Graphite using an Sb-Be Source," NAA-SR-9803 (August 1, 1964).

26. F. L. Fillmore, "Multigroup Calculation Methods with Application to the SGR Critical Experiments," NAA-SR-10531 (February 1, 1965).

27. D. C. Baller, "CAESAR, A Multigroup, One-Dimensional Diffusion Equation Code," NAA-SR-Memo-9423 (April 1963).

28. R. H. Shudde and J. Dyer, "TEMPEST II, A Neutron Thermalization Code," AI-64-Memo-186 (June 1962).

29. D. J. McGoff, "FORM, A Fourier Transform Fast Spectrum Code for the IBM-709," NAA-SR-Memo-5766 (September 1960); R. A. Blaine, "FORM," NAA-SR-Memo-9174 (November 1963).

30. W. K. Foell, "Diffusion Theory Studies of the ARMF Neutron Flux and Adjoint Function," MTR-ETR Technical Branches Quarterly Report, Oct 1 - Dec 31, 1963, IDO-16977 p 7-10 (May 1964).

31. N. C. Kaufman, "A Transport Study of the Neutron Flux, Adjoint, and Importance for the ARMF-II," IDO-17009 (September 1964).

32. E. P. Wigner et al., "Resonance Absorption of Neutrons by Spheres," J. Appl. Phys. 26, 260 (1955).

ACKNOWLEDGMENT

The authors wish to acknowledge the valuable contributions of J. F. Johnson to all phases of the experiments. Both sets of ovens used for the Doppler measurements were designed and developed primarily by P. J. Campbell and T. H. Springer. The authors are indebted to M. E. Rogers, G. Schumann, and O. R. Hillig for their assistance in preparing and performing the experiments. Profitable discussions of theory were held with A. R. Vernon and R. H. Sevy. L. S. Beller provided much useful information about his measurements on gold. Fruitful conversations about the results took place with D. Bogart and D. F. Shook.

Report Distribution List for Contract NAS3-7982

NASA Lewis Research Center (3)
21000 Brookpark Road
Cleveland, Ohio 44135
Attn: R. Sullivan, Program Manager
M.S. 49-2

NASA Lewis Research Center (1)
21000 Brookpark Road
Cleveland, Ohio 44135
Attn: Norman T. Musial

NASA Scientific and Technical (6 & repro.)
Information Facility
Box 5700
Bethesda, Maryland
Attn: NASA Representative

NASA Lewis Research Center (2)
21000 Brookpark Road
Cleveland, Ohio 44135
Attn: Library

NASA Lewis Research Center (1)
21000 Brookpark Road
Cleveland, Ohio 44135
Attn: Report Control Office

NASA Lewis Research Center (1)
21000 Brookpark Road
Cleveland, Ohio 44135
Attn: Report Control Office

NASA Lewis Research Center (1)
21000 Brookpark Road
Cleveland, Ohio 44135
Attn: Technical Utilization Office
Mail Stop 3-16

National Aeronautics and Space Administration (2)
Washington, D.C. 20546
Attn: Nuclear Propulsion Office

Manager (2)
Space Nuclear Propulsion Office
U. S. Atomic Energy Commission
Washington, D. C.
Attn: H. B. Finger

Space Nuclear Propulsion Office (1)
U. S. Atomic Energy Commission
Washington, D. C.
Attn: John Morrisey

U. S. Atomic Energy Commission (3)
Technical Reports Library
Washington, D. C.

U. S. Atomic Energy Commission (3)
Technical Information Service Extension
P.O. Box 62
Oak Ridge, Tennessee

NASA Lewis Research Center (1)
21000 Brookpark Road
Cleveland, Ohio 44135
Attn: Nuclear Rocket Technical
Mail Stop 501-2

NASA Lewis Research Center (1)
21000 Brookpark Road
Cleveland, Ohio 44135
Attn: Leroy B. Humble, MS 49-2

NASA Lewis Research Center (1)
21000 Brookpark Road
Cleveland, Ohio 44135
Attn: Samuel Kaufman, MS 49-2

NASA Lewis Research Center (1)
21000 Brookpark Road
Cleveland, Ohio 44135
Attn: Edward Lantz, MS 49-2

NASA Lewis Research Center (1)
21000 Brookpark Road
Cleveland, Ohio 44135
Attn: John Liwosz MS 501-2

NASA Lewis Research Center (1)
21000 Brookpark Road
Cleveland, Ohio 44135
Attn: Paul Klann, MS 49-2

NASA Lewis Research Center (1)
21000 Brookpark Road
Cleveland, Ohio 44135
Attn: Daniel Fieno, MS 49-2

NASA Lewis Research Center (1)
21000 Brookpark Road
Cleveland, Ohio 44135
Attn: Donald Shook, MS 49-2

NASA Lewis Research Center (1)
21000 Brookpark Road
Cleveland, Ohio 44135
Attn: Wendell Mayo, MS 49-2

NASA Lewis Research Center (1)
21000 Brookpark Road
Cleveland, Ohio 44135
Attn: Office of Reliability
and Quality Assurance

NASA Ames Research Center (1)
Moffett Field, California 94035
Attn: Library

NASA Flight Research Center (1)
P.O. Box 273
Edwards, California 93523
Attn: Library

NASA Goddard Space Flight Center (1)
Greenbelt, Maryland 20771
Attn: Library

Jet Propulsion Laboratory (1)
4800 Oak Grove Drive
Pasadena, California 91103
Attn: Library

NASA Langley Research Center (1)
Langley Station
Hampton, Virginia 23365
Attn: Library

NASA Manned Spacecraft Center (1)
Houston, Texas 77001
Attn: Library

NASA Marshall Space Flight Center (1)
Huntsville, Alabama 35812
Attn: Library

NASA Western Operations (1)
150 Pico Blvd.
Santa Monica, California 90406
Attn: Library

NASA Western Operations (1)
150 Pico Blvd.
Santa Monica, California 90406
Attn: L. Dondey

General Electric Company (1)
Nuclear Materials and Propulsion
Operations
P.O. Box 15132
Evendale, Ohio 45215
Attn: R. W. Briskin

Union Carbide Corporation (1)
Nuclear Division
P.O. Box X
Oak Ridge, Tennessee
Attn: R. C. Block

United Nuclear Corporation (1)
Development Division
5 New Street
White Plains, New York
Attn: D. Spielberg

Westinghouse Electric Corporation (1)
Astronuclear Laboratory
P.O. Box 10864
Pittsburgh 36, Pennsylvania

Aerojet General Nucleonics (1)
P.O. Box 77
San Ramon, California 94583
Attn: R. W. Durante

Argonne National Laboratory (1)
P.O. Box 299
Lemont, Illinois
Attn: J. F. Marchaterre
Project Manager, ANL
Nuclear Rocket Study

Brookhaven National Laboratory (1)
Upton, Long Island, New York
Attn: Dr. J. Stehn

General Atomic Division of General
Dynamics (1)
P.O. Box 6081
San Diego 12, California

Babcock & Wilcox Company (1)
Atomic Energy Division
1201 Kemper Street
P.O. Box 1260
Lynchburg, Virginia

Phillips Petroleum Company (1)
Research & Development Dept.
Atomic Energy Division
Idaho Falls, Idaho

Battelle Memorial Institute (1)
505 King Ave.,
Columbus, Ohio

General Electric Company (1)
Vallecitos Atomic Laboratory
Atomic Power Equipment Dept.
San Jose, California

Atomics International Division
North American Aviation
8900 DeSoto Ave.,
Canoga Park, California